Aqueous Ring-Opening Polymerization Induced Self-Assembly (ROPISA): Tailoring Anisotropic Nanoparticles Through Amino Acid N-Carboxyanhydrides (NCA) Monomer Selection

Hannah Beauseroy, Fatemeh Salimi, Julien Aujard-Catot, Léna Alembik, Sébastien Lecommandoux, Colin Bonduelle

Aqueous Ring-Opening Polymerization Induced Self-Assembly (ROPISA): Tailoring Anisotropic Nanoparticles Through Amino Acid *N*-Carboxyanhydrides (NCA) Monomer Selection

Hannah Beauseroy, Fatemeh Salimi, Julien Aujard-Catot, Léna Alembik, Sébastien Lecommandoux * and Colin Bonduelle *

University Bordeaux, CNRS, Bordeaux INP, LCPO, UMR 5629, F-33600 Pessac, France.

*: Corresponding author E-mails:

C.B. colin.bonduelle@enscbp.fr , ORCID: 0000-0002-7213-7861

S.L. lecommandoux@enscbp.fr , ORCID: 0000-0003-0465-8603

Abstract

The synthesis of anisotropic nanoparticles by polymerization-induced self-assembly (PISA) remains challenging yet holds significant potential for biomedical applications. In this context, aqueous ring-opening polymerization-induced self-assembly (ROPISA) of *N*-carboxyanhydrides (NCAs) has emerged as a promising strategy, offering a straightforward route to peptide-based nanomaterials. The present study was undertaken to evaluate the versatility of aqueous ROPISA across a range of NCAs, elucidating how their hydrophobicity and the chemical structure of the lateral chains provide access to nanoparticle anisotropy. A comparative analysis was conducted between NCAs with different protecting groups and those derived from distinct hydrophobic amino acids. Beyond hydrophobicity, the aqueous ROPISA of glycine NCA, phenylalanine NCA and tyrosine NCA revealed the crucial role of additional factors such as the hydrophilic/hydrophobic balance, π-π stacking interactions, and hydrogen bonding in shaping nanoparticle anisotropy. Overall, this work highlights the broad applicability of aqueous ROPISA across a wide range of NCA monomers and its ability to generate tailored anisotropic nanoparticles for advanced applications.

Introduction

Polymerization-induced self-assembly (PISA) has emerged as a highly versatile method in the field of dispersion polymerization, enabling the synthesis of well-defined nano-objects in a single-step process and at high concentrations.[1,2] The PISA process results in the formation of amphiphilic block copolymers that self-assemble *in situ*, leading to the generation of self-stabilized nanoparticles with diverse morphologies (*e.g.* spheres, worms, vesicles) eliminating the need for additional surfactants.[3–6] These morphologies can be controlled by modifying intrinsic parameters, including the chemical nature of the polymer segments,[7] the solvophilic/solvophobic ratio,[8,9] the architecture of the copolymer,[10,11] and the molar mass dispersity. Additionally, other important factors, including the solvent,[12] pH, salt concentration,[13,14] monomer concentration,[15] temperature,[16] stirring rate,[14] and initiator concentration can also influence the morphology of the nanoparticles.[17]

PISA has been proposed as a highly attractive method for the development of drug delivery systems (DDS) used in nanomedicine,[18–20] where size, dispersity and shape control are critical factors. Especially, the use of anisotropic nanoparticles (*i.e.,* nanoparticles with a length-to-width ratio greater than 1), although still relatively uncommon, shows great promise for further development of DDS. Indeed, several studies have demonstrated that anisotropic rod-like nanoparticles exhibit longer blood circulation half-life and enhanced cellular internalization compared to their isotropic spherical counterparts.[21–25] Despite this, the controlled formation of anisotropic nanoparticles using PISA remains limited to a narrow range of conditions that rely solely on hydrophilic to hydrophobic balance.[26] The PISA process has alternatively been extended to other supramolecular interactions, such as hydrogen bonding,[27] electrostatic interactions,[28] π-π interactions,[29] crystallization[30] and liquid crystal interactions.[31] This has enabled the formation of anisotropic nanostructures with larger aspect ratios.

The study of PISA has been predominantly conducted within the frameworks of reversible addition-fragmentation chain transfer (RAFT) polymerization,[32] atom-transfer radical polymerization (ATRP),[33] and nitroxide-mediated polymerization (NMP).[34] With these approaches, the scope of vinyl-based monomers that enable a PISA process in pure aqueous solutions remains restricted, and the majority of PISA processes require the use of organic solvents.[35,36] Moreover, PISA-based radical polymerization processes mostly result in vinyl-based nanomaterials constraining their applicability to further biomedical applications. For instance, the non-degradable nature of the nanomaterials raises concerns about toxic accumulation as they cannot be metabolized or excreted, potentially leading to adverse effects. This highlights the need for better control over the fate of nanoparticles *in vivo*, prompting the

design of fully (bio)degradable and biocompatible polymer assemblies. In this regard, the recent emergence of ring-opening PISA (ROPISA), of lactone,[37,38] cyclic carbonate,[39] amino acid *N*-carboxyanhydrides (NCA)[40,41] and *O*-carboxyanhydrides[42] offers promising new solutions.

We have recently reported a distinctive PISA process occurring in pure aqueous solutions that yields the formation of peptidic nanomaterials, the aqueous ROPISA of γ-benzyl-glutamate and leucine *N*-carboxyanhydrides (NCA).[41,43] Despite the sensitivity of NCA to moisture, the issue of monomer hydrolysis and subsequent uncontrolled polymerization[44,45] was addressed by adjusting the reaction conditions (pH and solids content) to allow for the ring opening by the amine propagating species to occur at a faster rate than hydrolysis due to micellization and confinement of the polymerization. In addition, the aqueous phase enabled the synthesis of protein-polymer conjugates and nanomaterials composed entirely of amino acids, and displaying protein-like properties.[46–48] As other PISA, the aqueous ROPISA of NCA is a process that enables anisotropic nanoparticles, the shape of which could be controlled by the chirality of the monomer and/or the secondary structure of the polypeptide block.[49] Nevertheless, only a limited number of monomers have been investigated so far,[47,49,50] and the conventional principles of PISA, such as varying the hydrophilic/hydrophobic block ratio or concentration to achieve diverse morphologies, seem not applicable in this context.

Herein, we explore the versatility of this approach by investigating the aqueous ROPISA of various NCA monomer structures displaying different hydrophobicity, π–π stacking and H-bonding interactions and ability to stabilize polypeptide conformation when polymerized (Scheme 1). First, the aqueous ROPISA of lysine monomers bearing different protecting groups (benzyloxycarbonyl, Z; trifluoroacetyl, TFA; and tert-butyloxycarbonyl, Boc) was studied and compared. We found that the choice of the protecting group for an amino acid could be means of influencing the anisotropy by promoting good monomer dispersion, hydophobicity and π–π stacking during the propagation. Subsequently, to gain insight into the influence of side chain hydrophobicity, glycine, alanine, leucine and phenylalanine NCAs were subjected to further investigation. Interestingly, all these monomers produced anisotropic nanomaterials, and we clearly observed that varying hydrophobicity but also π-π stacking or H-bonding ability impacted the kinetic of the ROP and the aspect ratio of the resulting nanomaterials. Finally, and to specifically decipher the influence of the π-π stacking, the polymerization of phenylalanine NCA and tyrosine NCA, both emerging amino acid to design DDS,[51] were subjected to a comprehensive study. With these two monomers, we confirmed that the tuning of anisotropy is not only driven by the hydrophobicity of the monomer alone, but also by the π-π stacking interactions of the side chains and the overall

hydrophilic/hydrophobic ratio. Altogether, our results highlight the versatility of aqueous ROPISA in designing anisotropic nanoparticles, a morphology achievable with numerous NCA monomers (eight in this study). Moreover, side-chain functionalities serve as a key leverage to fine-tune the length-to-width ratio and rigidity.

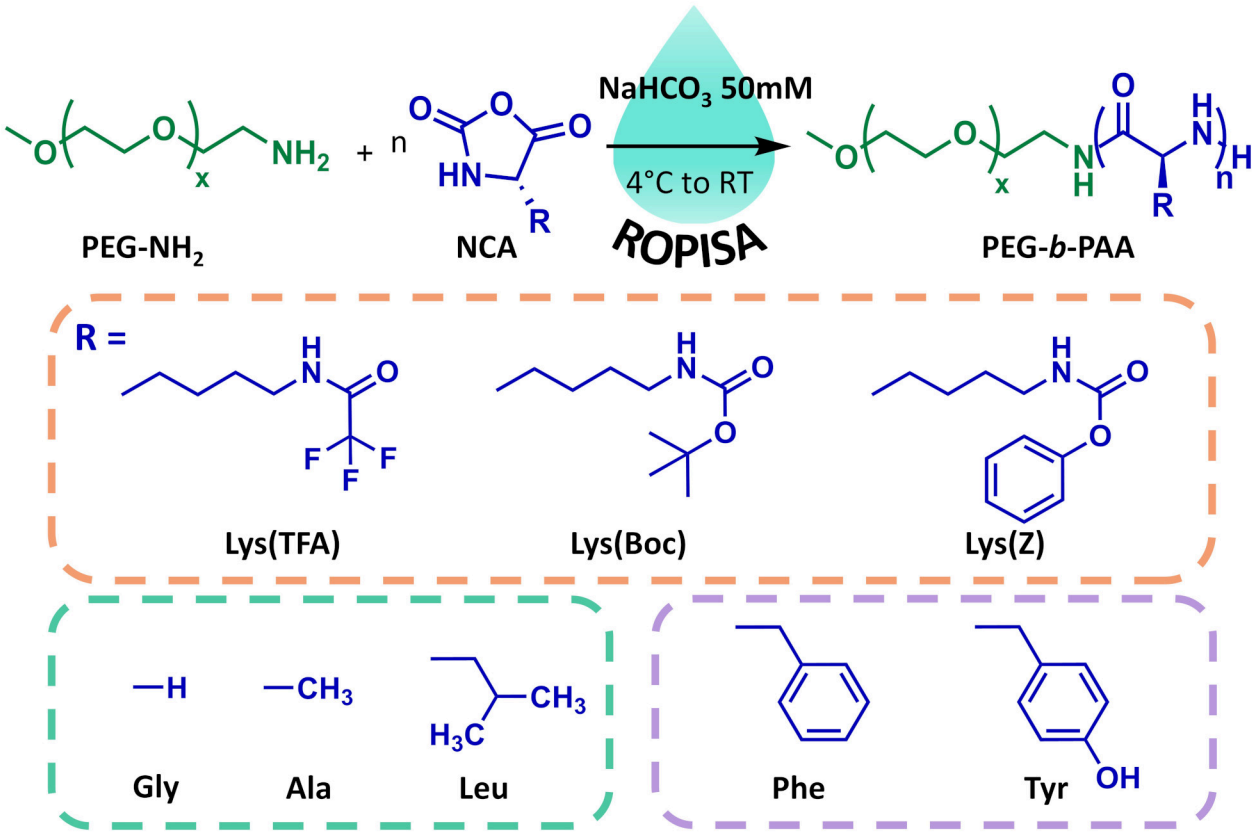

Scheme 1. Schematic representation of aqueous ring-opening polymerization induced self-assembly (ROPISA) with a range of amino acid *N*-carboxyanhydrides used as monomers (in orange, influence of the protecting group; in green, influence of the hydrophobicity and in purple, influence of the π–π stacking).

Results and discussion

ROPISA is influenced by the chemical nature of the protecting groups

Although recent advances in ROP have enabled the rapid generation of polypeptides with predictable molar masses (M_n), low dispersity ($Đ$), and well-defined reactive end group, the synthesis of NCA monomers and their polymerization usually requires the use of organic solvents and therefore, amino acids units with protected side chains.[52] We first investigated the influence of protecting groups with varying steric hindrance and water solubility on the aqueous ROPISA of three lysine-derived NCA monomers, all known to stabilize similar conformations: ε-trifluoroacetyl-*L*-lysine-NCA

(Lys(TFA)-NCA) , ε-tert-butyloxycarbonyl-*L*-lysine-NCA (Lys(Boc)-NCA)) and ε-benzyloxycarbonyl-*L*-lysine-NCA (Lys(Z)-NCA).[53] The aqueous ROPISA was conducted for each monomer using α-amino-poly(ethylene glycol) (PEG5k-NH_2) as the macro-initiator in an ice-cold aqueous sodium bicarbonate solution (pH 8.5, 50 mM) with 20 equivalents of NCA monomer, under vigorous stirring conditions. In all three cases, the NCA monomers were fully converted in a few hours, as evidenced by ^{1}H NMR spectroscopy and SEC chromatography. The resulting SEC chromatograms exhibited a monomodal distribution with narrow molar mass dispersity values, and the retention times shifted to lower values compared to the PEG macroinitiator, confirming effective block extension. Moreover, ^{1}H NMR spectra indicated that block copolymers exhibited similar degree of polymerization (DP) values ranging from 22 to 24 (see **Table 1, Figure 1, Figure S1-S3**). Following dialysis against water to remove salts, the nanomaterial suspensions were characterized using microscopy and light scattering techniques. Dynamic light scattering (DLS) analyses revealed the presence of nanoparticles with Z-average diameters of 101 nm for **PEG_{5k}-*b*-PLys(Z)$_{20}$**, 92 nm for **PEG_{5k}-*b*-PLys(Boc)$_{20}$** and 114 nm for **PEG_{5k}-*b*-PLys(TFA)$_{20}$**, with polydispersity index values of 0.15, 0.38 and 0.21 respectively (**Table 1, Figure S4**). In the case of nanomaterials with anisotropic shape, the Z-average diameter provided by DLS is only equivalent to that of a sphere, which can be misleading for particles that are not spherical. This anisotropic shape was indeed revealed by imaging the opalescent solutions obtained upon ROPISA using transmission electron microscopy (TEM). For the three NCA monomers, the microscopy images established the presence of flexible, worm-like nanoparticles (**Figure 1**) and approximately fifty nanoparticles were randomly selected and compared to statistically analyze the length and width of the nanomaterials (**Figure S5**).

Table 1. Macromolecular characteristics of diblock copolymers obtained by aqueous ROPISA with different monomers, using α-amino poly(ethylene glycol) as macroinitiator, at a feeding ratio of 20.

[a)] Number average molar-mass (M_n) and molar-mass dispersity determined by SEC in DMF +1% LiBr using PS calibration, [b)] in HFIP+0.05% KTFA using PMMA calibration [c)] Number average molar-mass (M_n) and degree of polymerization (DP)

Copolymer	Monomer	Theory	SEC		^{1}H NMR		Yield (%)	DLS
		M_n [g.mol^{-1}]	M_n [g.mol^{-1}]	$Đ$	M_n [g.mol^{-1}]	DP		D_Z [nm] (σ) [e)]
PEG$_{5k}$-*b*-PLys(TFA)$_{20}$	*L*-*NTFA*Lys	9 200	13 100 [a)]	1.06 [a)]	10 400 [c)]	24 [c)]	77	114 ± 2 (0.21 ± 0.01)
PEG$_{5k}$-*b*-PLys(Boc)$_{20}$	*L*-*NBoc*Lys	9 400	12 100 [a)]	1.05 [a)]	10 000 [c)]	22 [c)]	82	92 ± 3 (0.38 ± 0.04)
PEG$_{5k}$-*b*-PLys(Z)$_{20}$	*L*-*NZ*Lys	9 900	13 900 [a)]	1.12 [a)]	10 800 [c)]	22 [c)]	92	101 ± 2 (0.15 ± 0.02)
PEG$_{5k}$-*b*-PGly$_{20}$	Gly	6 100	49 100 [b)]	1.07 [b)]	6 400 [d)]	25 [d)]	56	265 ± 8 (0.53 ± 0.02)
PEG$_{5k}$-*b*-PAla$_{20}$	*L*-Ala	6 400	33 600 [b)]	1.07 [b)]	6 500 [d)]	21 [d)]	73	149 ± 1 (0.41 ± 0.03)
PEG$_{5k}$-*b*-PLeu$_{20}$	*L*-Leu	7 200	9 200 [a)]	1.03 [a)]	7 400 [d)]	21 [d)]	90	101 ± 2 (0.34 ± 0.05)
PEG$_{5k}$-*b*-PPhe$_{20}$	*L*-Phe	7 900	9 000 [a)]	1.03 [a)]	8 200 [d)]	22 [d)]	79	85 ± 1 (0.27 ± 0.02)
PEG$_{5k}$-*b*-PTyr$_{20}$	*L*-Tyr	8 200	9 400 [a)]	1.07 [a)]	7 600 [c)]	16 [c)]	89	77 ± 4 (0.23 ± 0.1)

determined by ^{1}H NMR in DMSO-d$_6$, [d)] in TFA-*d*, [e)] Hydrodynamic diameter (D_Z) and polydispersity (σ) determined by DLS at 90°.

Remarkably, anisotropic nanoparticles were obtained with all 3 monomers. TEM imaging with **PEG$_{5k}$-*b*-PLys(TFA)$_{20}$** exhibited a coexistence of spherical micelles and necklace-type nanoparticles with a total mean length of 59 ± 37 nm, and a width of 21 ± 4 nm, while in TEM imaging of **PEG$_{5k}$-*b*-PLys(Boc)$_{20}$** suspensions, long and thick worm-like nanoparticles were observed, with a mean length of 116 ± 43 nm, and a width of 30 ± 5 nm. As already reported by *Liu* et al.,[49] TEM imaging of **PEG$_{5k}$-*b*-PLys(Z)$_{20}$**, displayed homogeneous superhelix type nanoparticles of 173 ± 80 nm length and 38 ± 7 nm width. Overall, the DLS results and TEM imaging indicated that nanoparticles formed with the Z protecting group are longer and thicker than those with the tert-butyl carbamate (Boc) protecting group, and more homogeneous than those with the trifluoroacetyl (TFA) one. As has been previously established, the influence of the secondary structure is an important factor that may guide the anisotropy upon ROPISA,[43] and to further elucidate this influence, we analyzed the lyophilized powder obtained with the 3 different monomer units using ATR-FTIR spectroscopy (see **Figure S6**).

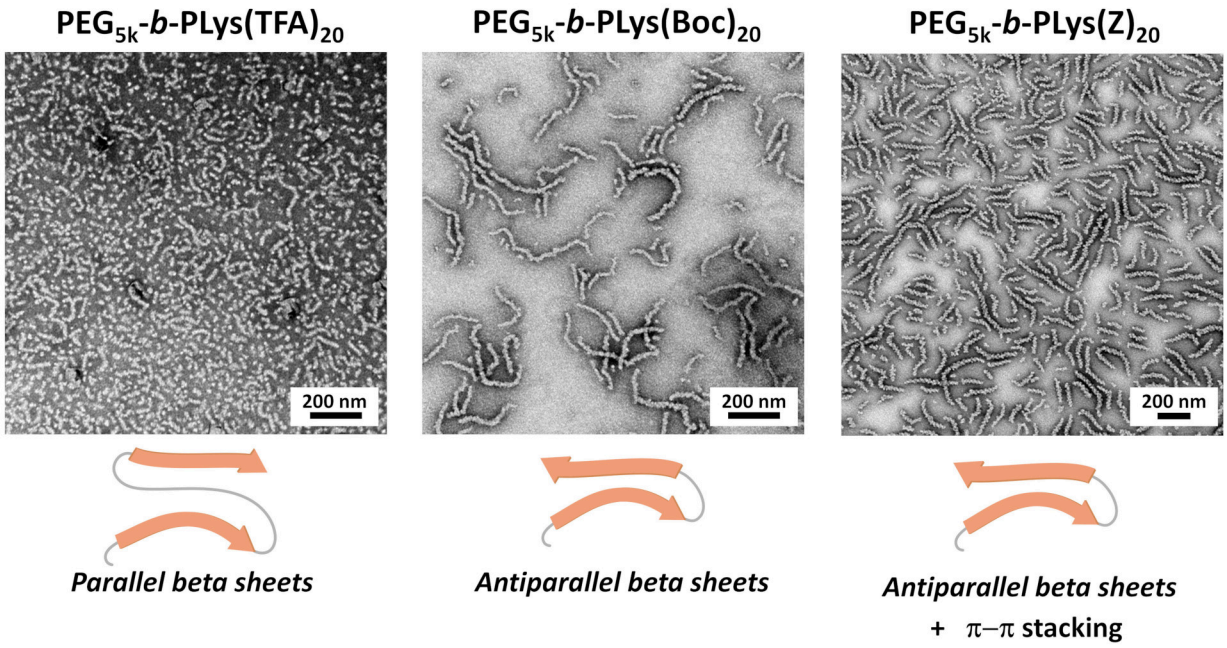

Figure 1. Representative TEM images of the different copolymer nanoparticles obtained with Lys(TFA), Lys(Boc), Lys(Z) at an initial [M]/[I] ratio of 20, initiated by PEG_{5k}-NH_2, with corresponding parameters influencing the anisotropy.

With both Boc and Z protecting groups, the spectra demonstrated the presence of a prominent peak at 1630 cm^{-1}, which was attributed to the amide I and associated to a peak at 1530 cm^{-1} (the amide II region), along with a peak at 1690 cm^{-1} (side chain carbonyl). These stretching corroborated the presence of an antiparallel β-sheet structure, a conformation that was previously associated to the formation of ribbon-like nanostructures.[49] In our ROPISA conditions, no notable differences in conformation were observed between the Boc and Z protecting groups. However, the anisotropic shapes of the nanomaterial exhibited significant variation (116 nm *versus* 173 nm) that we attributed to the π-π stacking introduced with Z. With TFA protecting groups, the ATR-FTIR spectra revealed that the amide I region exhibited a prominent peak at 1625 cm^{-1}, while the amide II region displayed peaks at 1555 cm^{-1} and 1540 cm^{-1}. These findings suggest that this last β-sheet structure was more constrained (*i.e.,* parallel β-sheet), which resulted in less pronounced anisotropy. Overall, the present study demonstrated that besides the secondary structure, the dimension (parallel/antiparallel) and the chemical nature of the protecting group (π-π stacking) were also key parameters modulating the anisotropy.

To further investigate the influence of the overall hydrophilic/hydrophobic ratio with the 3 lysine derivatives, various aqueous ROPISA were implemented using different feeding ratios (*e.g.*, initial [M]/[I] from 10 to 40) and α-amino-poly(ethylene glycol) (PEG_{5k}-NH_2) as the macro-initiator.

The results of the ^{1}H NMR spectroscopy performed upon ROPISA indicated that the **PEG$_{5k}$-*b*-PLys(Z)** block copolymers exhibited degree of polymerization (DP) values ranging from 15 to 44, which were in close agreement with the targeted values (**Table S1, Figure S1**). The corresponding SEC chromatograms exhibited a monomodal distribution with narrow molar mass dispersity values, and the retention times shifted to lower values compared to the PEG macroinitiator, confirming effective block extension (**Erreur ! Source du renvoi introuvable.a).** DLS analysis revealed a progressive increase in the size of the nanoparticles (**Figure S7**) while TEM imaging showed the formation of heterogeneous helical ribbons for PEG$_{5k}$-*b*-PLysZ$_{10}$. However, with increasing Lys(Z) block length, larger aggregates were observed. Overall, anisotropic morphologies were obtained at specific hydrophilic/hydrophobic ratios, but increasing the length of the hydrophobic block resulted in uncontrolled aggregation. This highlights the critical balance needed in tuning block copolymer composition to achieve well-defined self-assembled structures with the ROPISA of Lys(Z)-NCA.

In the absence of π-π stacking stabilization, the aqueous ROPISA of Lys(TFA)-NCA also led to the formation of copolymers whose degree of polymerization (DP) as determined by ^{1}H NMR was found to be in agreement with the theoretical values (see **Table S1, Figure S2**). However, beyond M/I = 20, SEC profiles (**Erreur ! Source du renvoi introuvable.b**) exhibited peak splitting, which correlated with increasing molar mass and the emergence of a peak at lower molar masses. This phenomenon suggested the formation of an oligomeric population generated through residual hydrolysis of NCA monomers ("water-initiated"). This was attributed to less efficient dispersion of the NCA monomer in the aqueous phase that could originate from the strong hydrophobic nature of TFA. Finally, the aqueous ROPISA of Lys(Boc)-NCA, displaying more steric hindrance than the two other lysine derivatives, led to the formation of copolymers whose degree of polymerization (DP) calculated by ^{1}H NMR indicated that the molar masses remained unchanged at increasing feeding ratio (see **Erreur ! Source du renvoi introuvable.c**, **Table S1, Figure S3**). Moreover, the SEC profiles exhibited an increased number of oligomers formed through water initiation, suggesting that the polypeptide chains were unable to maintain an optimal propagation rate during ROPISA. Overall, comparing the aqueous ROPISA of Lys(TFA)-NCA, Lys(Boc)-NCA, and Lys(Z)-NCA, demonstrated that the hydrophobicity of the different protecting groups significantly influenced the polymerization process and the anisotropy. At higher [M]/[I], water initiation was observed with Lys(TFA)-NCA and Lys(Boc)-NCA. Moreover, we found that the benzyl group facilitated a superior dispersion of the monomer powder in the aqueous medium and favored a more pronounced anisotropic shape through π-π stacking. All these factors, in turn, enable a more regulated aqueous polymerization and self-

assembly for Lys(Z)-NCA, which results in a more uniform distribution of nanoparticles than that observed with Boc- and TFA-protected groups.

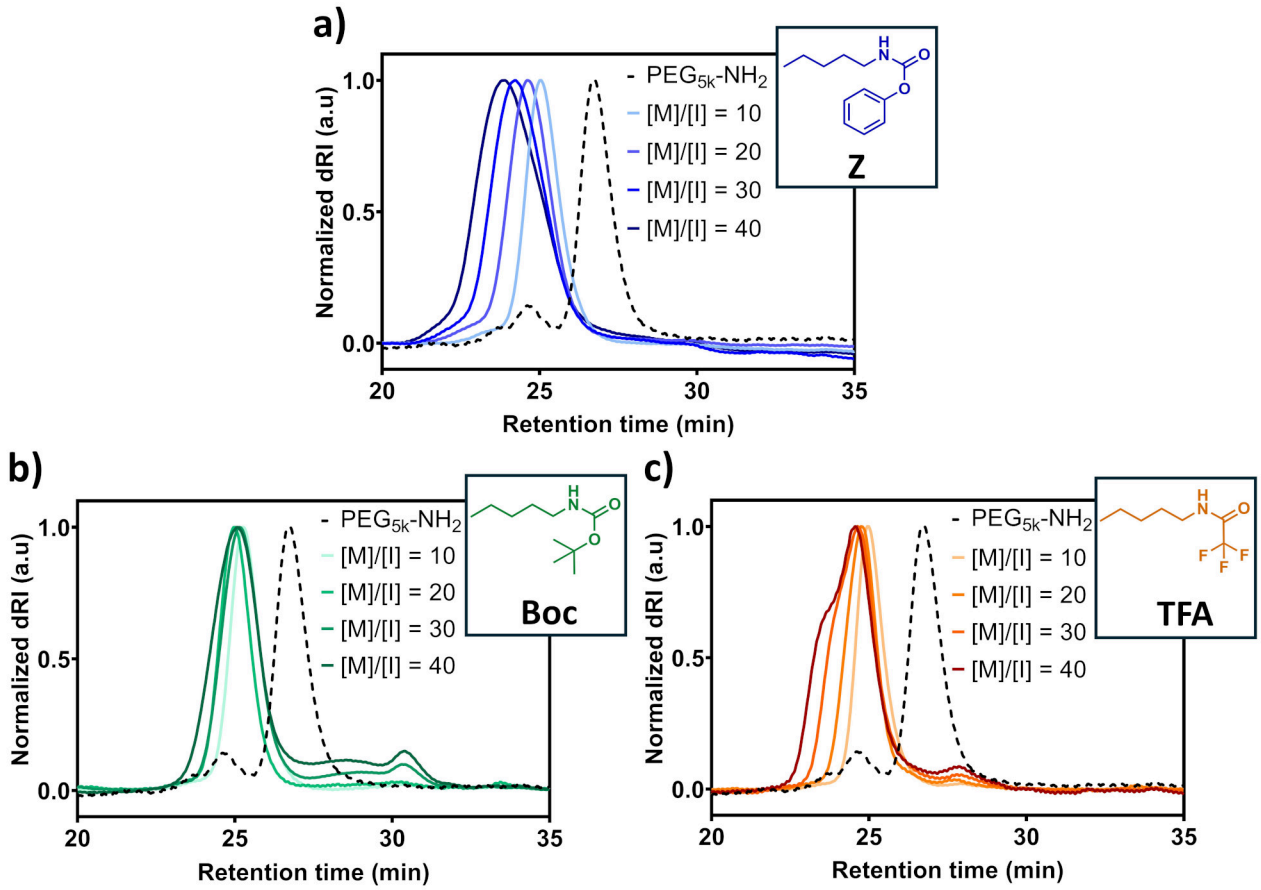

Figure 2. Size exclusion chromatograms of (a) **PEG$_{5k}$-*b*-PLys(Z)$_n$**, (b) **PEG$_{5k}$-*b*-PLys(Boc)$_n$** and (c) **PEG$_{5k}$-*b*-PLys(TFA)$_n$** with targeted DP of 10, 20, 30 and 40 in DMF + 1% LiBr (The peaks observed at lower mass, below the macroinitiator, were attributed to water-initiated ROP).

ROPISA is influenced by the hydrophobicity of the amino-acid side chain

The study of the lysine derivatives with different protecting groups clearly showed that the hydrophobicity of the side chain can play an important role in the ROPISA process and modulate the anisotropy of the nanoparticles that are obtained. To better evaluate this influence, we selected a series of 5 NCA monomers, Glycine-NCA, Alanine-NCA, Tyrosine-NCA, Leucine-NCA, and Phenylalanine-NCA, arranged in order of increasing hydrophobicity, with calculated Log P_{oct} values of -0.31, 0.02, 1, 1.33 and 1.48 respectively.[54–56] Alanine NCA (Ala-NCA) was synthesized by the Leuchs method (see **Figure S8**), while the others were commercially available. The aqueous polymerization was carried out under the same

conditions as those previously used with lysine derivatives, with an initial feed ratio [M]/[I] of 20. According to ^{1}H NMR spectroscopy, the different ROPISA afforded copolymers with DP values similar to the targeted ones (**Table 1**, **Figure S9-S13**). SEC analyses demonstrated that well-defined amphiphilic block copolymers with a narrow dispersity ($Đ$ < 1.2) were consistently produced, confirming the effectiveness of the aqueous ROPISA at low [M]/[I] for all hydrophobic monomers and surprisingly, even for the non-hydrophobic monomer Glycine-NCA (**Table 1, Figure S14-S18**).

Following dialysis to remove salts, the suspensions of nanoparticles were analyzed by DLS and imaged by TEM. For **PEG$_{5k}$-*b*-PGly$_{20}$**, DLS showed sizes with high dispersity ($\sigma \approx 0.5$) (**Figure S19**), likely due to the nanoparticles' morphology. Indeed, TEM images revealed the presence of flexible fibrils, both simple and branched, with an average diameter of 13 ± 2 nm (**Figure 3, Figure S20**). The length of these fibrils could not be determined because of the variability in branching. It is important to note that the glycine monomer was fully soluble at the initial stage of the ROPISA process and that the aggregation of the polypeptide is attributable to its ability to form intermolecular hydrogen bond and other dipolar interactions such as CO–CO interactions.[57] Interestingly, the sphere-equivalent Z-average diameter of the nanoparticles suspensions was found to be larger for **PEG$_{5k}$-*b*-PAla$_{20}$** than for **PEG$_{5k}$-*b*-PLeu$_{20}$,** although the dispersity was high ($\sigma > 0.2$) in both cases (**Table 1, Figure 3, Figure S21, S22**). For both NCA monomers, TEM revealed the presence of long, thin, and rigid rod-like nanoparticles with homogeneous diameters (151 ± 58 nm in length and 11 ± 2 nm diameter for **PEG$_{5k}$-*b*-PAla$_{20}$**; 102 ± 42 nm in length, 11 ± 2 nm diameter for **PEG$_{5k}$-*b*-PLeu$_{20}$**, **Figure 3**, **Figure S23, S24**). **PEG$_{5k}$-*b*-PAla$_{20}$** nanoparticles had a higher aspect ratio than **PEG$_{5k}$-*b*-PLeu$_{20}$** nanoparticles. Nanoparticles suspensions prepared from **PEG$_{5k}$-*b*-PPhe$_{20}$** exhibited a sphere-equivalent z-average diameter distribution that was more homogenous, with a mean diameter of 85 ± 1 nm and a polydispersity index (σ) of 0.27 ± 0.02 (**Table 1**, **Figure S25**). However, in marked contrast to the findings reported by *Morrel* et al. using a polysarcosine macroinitiator,[47] we observed by TEM a heterogeneous mixture of long, thick and rigid nanorods with spherical micelles. The distribution of nanoparticles was rather heterogenous in length (105 ± 82 nm), but the dispersion of diameters was narrow (26 ± 4 nm) (**Figure S26**).

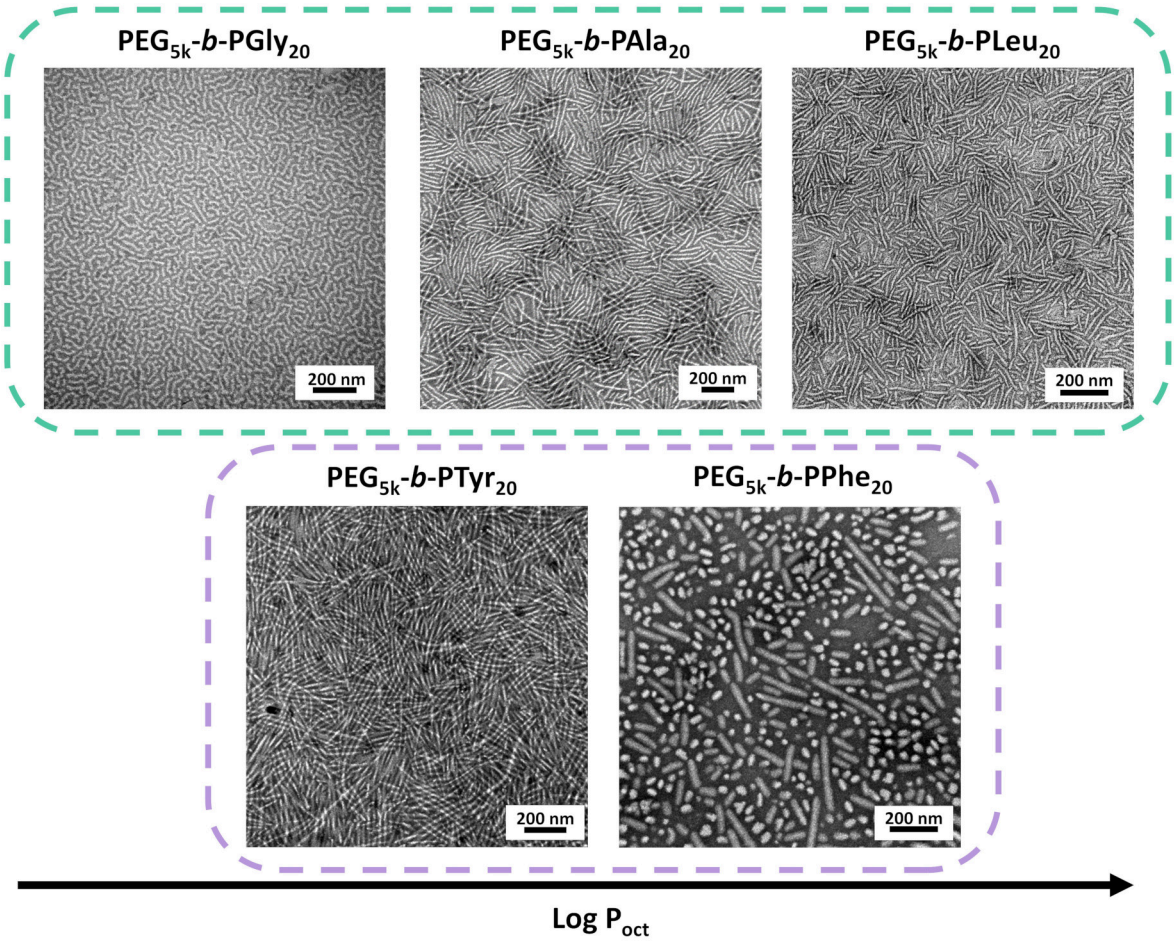

Figure 3. Representative TEM images of the different copolymer nanoparticles obtained with Gly, Ala, Leu, Phe and Tyr at an initial [M]/[I] ratio of 20, initiated by PEG_{5k}-NH_2. In green, influence of the hydrophobicity and in purple, influence of the π–π stacking, with increasing Log P_{oct}.

Finally, DLS analyses of **PEG_{5k}-*b*-$PTyr_{20}$**, indicated a Z-average hydrodynamic diameter of 77 ± 4 nm (**Figure S27**). In comparison to **PEG_{5k}-*b*-$PPhe_{20}$**, this ROPISA yielded nanoparticles with a smaller diameter and a significantly lower proportion of spherical micelles as shown by TEM (**Table 1, Figure 3, Figure S28).**

Beyond hydrophobicity, the influence of the secondary structure is an important factor that may also guide the anisotropy of the proposed 5 monomers. To further elucidate this influence, we also analyzed the lyophilized powder obtained upon ROPISA using ATR-FTIR spectroscopy. First, glycine, the simplest and achiral amino acid, lacks the classic structural features of typical polypeptides affording secondary structure. However, glycine's specific conformational structure involving hydrogen bonding have already been reported and found similar to beta sheets.[58,59] The spectrum displayed a prominent peak in the amide I region at 1644 cm^{-1} and another in the amide II region at 1560 cm^{-1}, which are characteristic of the

poly(glycine II) (PGII) conformation—an extended helical structure commonly found in solution (**Figure S29**).[58,60] In comparison, the FTIR spectrum of **PEG$_{5k}$-*b*-PAla$_{20}$** showed a peak at 1625 cm^{-1} in the amide I region and at 1538 cm^{-1} in the amide II region, indicating a β-sheet conformation. For **PEG$_{5k}$-*b*-PLeu$_{20}$**, a prominent peak at 1627 cm^{-1} and a smaller one at 1653 cm^{-1} in the amide I region, along with a peak at 1544 cm^{-1} in the amide II region, suggest a mix of β-sheet and α-helical structures (**Figure S30**). For all 3 monomers, the "β-sheet" conformation was likely responsible for the increased rigidity observed particularly comparing alanine and leucine. FTIR analyses were also conducted on dried powders of **PEG$_{5k}$-*b*-PPhe$_{20}$** and **PEG$_{5k}$-*b*-PTyr$_{20}$** (**Figure S31**). The phenylalanine-based copolymer displayed a peak at 1632 cm^{-1} in the amide I region and at 1545 cm^{-1} in the amide II region, indicative of β-sheet structures. Similarly, the tyrosine-based copolymer exhibited characteristic peaks in both the amide I and amide II regions, also confirming the presence of β-sheet conformations. The observed anisotropic structures likely arise from the combined effects of hydrophobic interactions and the intrinsic β-sheet secondary structure of the polypeptides. The β-sheet conformation provides a rigid and directional framework, while the degree of hydrophobicity modulates the overall rigidity and prominence of the anisotropy.

Recent studies carried out in organic solvents and with lactide suggested that the ROPISA process may be strongly influenced by ROP kinetics and that the speed of these kinetics, compared with self-assembly kinetics involving a CDSA process, may explain the formation of more anisotropic morphologies.[74] To better understand such influence, aqueous ROPISA kinetics were studied by monitoring the different monomer conversion using ^{1}H NMR at a feed-ratio of 20 and initiated by PEG$_{5k}$-NH$_2$. HCl was used to quench polymerization at different timepoints (**Figure S32-S36**). Remarkably, in the case of glycine and alanine, the aqueous ROP was "superfast" and achieved in less than 5 minutes. Plots of ln ([M]$_0$/[M]$_t$) versus time indicated a first-order dependence on the monomer concentration (**Figure 4**). A detailed investigation of polymerization kinetics yielded an apparent kinetics rate constant (k) value of 1.52 min^{-1} and 1.535 min^{-1} respectively. The k values with the use of leucine, phenylalanine and tyrosine NCAs were found slightly higher with values of 0.286 min^{-1}, 0.152 min^{-1} and 0.004 min^{-1} respectively. This kinetic study indicates that the aqueous ROP kinetics are directly influenced by the hydrophobicity of the NCA monomer. Hypothetically, the more hydrophobic the monomer, such as Phenylalanine-NCA, the slower the dispersion and diffusion of the solid-state In addition, consistent with previous studies on the ROPI-CDSA of lactide, slower ROP kinetics observed with Phenylalanine-NCA and Tyrosine-NCA may lead

to reduced anisotropy. This could explain the coexistence of spherical and rod-like nanoparticles for these monomers.

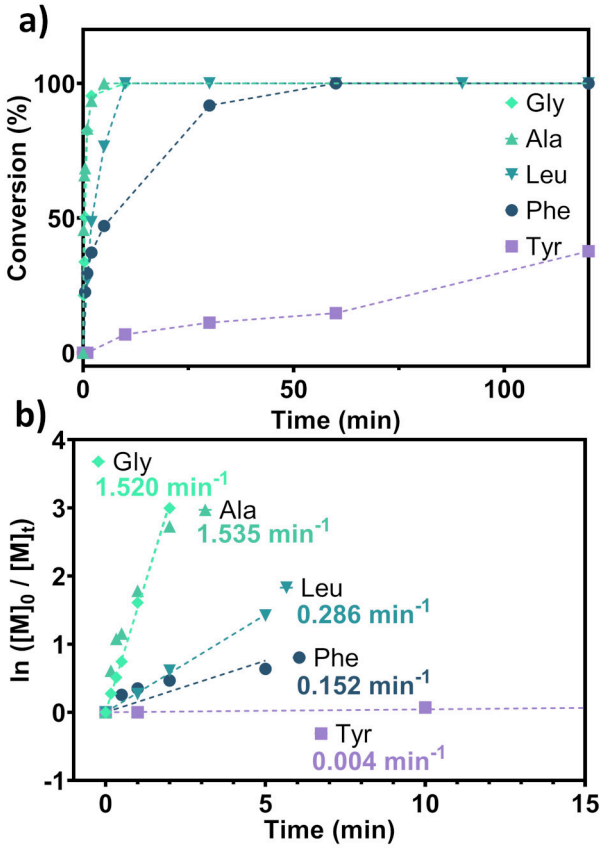

Figure 4. Kinetic profiles of (a) conversion vs time and (b) $\ln([M]_0/[M]_t)$ vs time at an initial [M]/[I] ratio of 20 determined by ^{1}H NMR spectra.

In summary, aqueous ROPISA enables the polymerization of diverse NCA monomers with varying hydrophobicity. The hydrophobicity, chemical structure, and steric hindrance of these monomers significantly influence polymerization kinetics and self-assembly behavior. In contrast to classical dispersion methods, such as RAFT-PISA in water, which impose limitations on the available monomers, ROPISA appears to exhibit a wider range of monomer options. In RAFT-PISA, the hydrophobicity of core-forming monomers and their corresponding oligomers requires careful control.[35] In contrast, aqueous ROPISA accommodates a wider range of hydrophobic monomers, as long as they are sufficiently dispersed to diffuse into the polymerization locus.

Besides hydrophobicity, π-π interactions versus hydrophilic content : Phenylalanine NCA

Our previous studies[41,46] and the current investigation indicate that the majority of our ROPISA attempts result in the formation of anisotropic nanomaterials, in marked contrast to other PISA processes. Nevertheless, nanoparticles solutions comprising **PEG$_{5k}$-*b*-PPhe$_{20}$** and **PEG$_{5k}$-*b*-PTyr$_{20}$** also exhibited the simultaneous formation of spherical micelles during ROP. This difference can be attributed to slower ROP kinetics, which are not amenable to a CDSA process, as shown by recent studies on lactide.[61] Indeed, the presence of spherical shapes suggests that self-assembly is closer to an equilibrium in which the amphiphilic character may have more influence. To determine whether morphology could be influenced by the hydrophilic/hydrophobic ratio, we further investigated the ROPISA of Phe-NCA by varying the M/I ratio. The objective was also to decipher how the aromatic ring of the side chain of phenylalanine could arrange stabilizing π-π interactions that are especially relevant in drug delivery applications.[62,63] So far, the traditional ring-opening polymerization performed in organic solvent still presents significant challenges when used to polymerize Phe-NCA and this monomer has been mainly studied in copolymerization systems.[64–66] In a non-aqueous ROPISA approach, *Du* et al. investigated the fate of Phe-NCA in THF, initiated by PEG$_{2k}$-NH$_2$, and achieved the formation of polymersomes with a block ratio of 1:20 and a solid content of 20%.[40] Subsequently, *Morrel* et al. employed aqueous ROP to extend polysarcosine with Phe-NCA, with the objective of synthesizing a polymer with DP ranging from 8 to 33. In this second case, the process also resulted in nanomaterials exhibiting anisotropic characteristics.[47]

We first performed the aqueous ROPISA of Phe-NCA, utilizing a 2kDa PEG amine macroinitiator, with the aim of targeting lower hydrophilic fractions than the one already studied (**Figure 3**). The monomer powder was combined with the initiator using extensive stirring at 4°C and in sodium bicarbonate aqueous buffer (pH 8.5, 50 mM) at a monomer-to-initiator ratio of 2 (f_{PEG} of 0.6, **PEG$_{2k}$-*b*-PPhe$_2$**), 5 (f_{PEG} of 0.5, **PEG$_{2k}$-*b*-PPhe$_5$**), 10 (f_{PEG} of 0.4, **PEG$_{2k}$-*b*-PPhe$_{10}$**) and 20 (f_{PEG} of 0.3, **PEG$_{2k}$-*b*-PPhe$_{20}$**) and at a solid content of 7 wt%. Upon ROPISA, the solutions were dialyzed against ultra-pure water (RC cut-off 1kDa) for 2 days, with regular changes of water. NMR analyses confirmed the expected chemical structures and enabled the estimation of number-averaged molar mass M_n values that were slightly higher than the targeted values (**Table 2, Figure S37**). Furthermore, the chain extension proceeded effectively, as demonstrated by the SEC chromatograms and corroborated by the low molar mass dispersity ($Đ$) values between 1.05 and 1.07 (**Figure 5A**). Following dialysis, the nanomaterial suspensions were characterized using microscopy and light scattering techniques.

Nanoparticle formation was confirmed by DLS and TEM analyses, even at a DP of 8, with a mixture of short rod and aggregate structures (**Figure 6, Figure S38**). As the length of the polypeptide block increased, the nanoparticles developed into progressively longer and more elongated structures at DP of 11. At a DP of 15, the nanoparticles exhibited enhanced rigidity, and at a DP of 20, they formed aggregates (**Figure 6**). To enhance the hydrophilic/hydrophobic ratio and examine its influence on the resulting nanoparticle morphology, we proceeded to conduct the aqueous ROPISA of Phe-NCA with the incorporation of 5 kDa or 10 kDa PEG amine (f_{PEG} between 0.6 and 0.9, **Table 2**). The macroinitiator was combined with the monomer powder through extensive stirring at 4°C and in a sodium bicarbonate aqueous buffer (pH 8.5, 50 mM) at a monomer-to-initiator ratio ranging from 2 to 20. In all instances, the NCA monomers underwent complete conversion, as substantiated by ^{1}H NMR spectroscopy. Additionally, ^{1}H NMR spectroscopy and SEC chromatograms demonstrated effective control over the polymerization process. The calculated DP values by ^{1}H NMR exhibited a high degree of correlation with the targeted values, as evidenced by the data presented in **Erreur ! Source du renvoi introuvable.** (**Figure S11, S39, S40**).

Table 2. Macromolecular characteristics of diblock copolymers obtained by aqueous ROPISA with Phe-NCA.

Copolymer	Theory	SEC	^{1}H NMR	Yield (%)	DLS

	M_n [g.mol^{-1}]	M_n [g.mol^{-1}] [a]	$Đ$ [a]	M_n [g.mol^{-1}] [c]	DP [c]	f_{PEG} [d]		D_Z [nm] (σ) [e]
PEG$_{2k}$-*b*-PPhe$_2$	2 300	3 900	1.07	3 200	8	0.62	9	-
PEG$_{2k}$-*b*-PPhe$_5$	2 800	3 900	1.05	3 600	11	0.55	50	113 ± 1 (0.27 ± 0.01)
PEG$_{2k}$-*b*-PPhe$_{10}$	3 500	4 100	1.05	4 200	15	0.48	86	102 ± 1 (0.26 ± 0.02)
PEG$_{2k}$-*b*-PPhe$_{20}$	4 900	ns [b]	ns [b]	5 100	21	0.39	81	715 ± 55 (0.21 ± 0.16)
PEG$_{5k}$-*b*-PPhe$_2$	5 300	7 000	1.07	5 300	2	0.94	58	135 ± 5 (0.27 ± 0.01)
PEG$_{5k}$-*b*-PPhe$_5$	5 700	7 400	1.07	5 800	5	0.87	65	82 ± 2 (0.25 ± 0.01)
PEG$_{5k}$-*b*-PPhe$_{10}$	6 400	7 900	1.07	6 500	10	0.77	74	87 ± 1 (0.2 ± 0.01)
PEG$_{5k}$-*b*-PPhe$_{20}$	7 900	9 000	1.03	8 200	22	0.61	79	85 ± 1 (0.27 ± 0.02)
PEG$_{10k}$-*b*-PPhe$_2$	10 300	18 400	1.02	10 400	3	0.96	82	253 ± 4 (0.48 ± 0.06)
PEG$_{10k}$-*b*-PPhe$_5$	10 800	19 900	1.03	11 000	7	0.91	95	66 ± 2 (0.38 ± 0.04)
PEG$_{10k}$-*b*-PPhe$_{10}$	11 500	19 900	1.03	11 500	10	0.87	76	80 ± 1 (0.37 ± 0.02)
PEG$_{10k}$-*b*-PPhe$_{20}$	12 900	ns [b]	ns [b]	13 700	25	0.73	84	118 ± 1 (0.23 ± 0.04)

[a] Number average molar-mass (M_n) and molar-mass dispersity determined by SEC in DMF +1% LiBr using PS calibration, [b] not soluble in common SEC solvents, [c] Number average molar-mass (M_n) and degree of polymerization (DP) determined by ^{1}H NMR in in TFA-*d*, [d] Hydrophilic fraction or PEG fraction determined by this equation $\frac{M_n \text{ PEG}}{M_n \text{ copolymer}}$ with M_n from ^{1}H NMR. [e] Hydrodynamic diameter (D_Z) and polydispersity (σ) determined by DLS at 90°.

SEC analysis confirmed the effective extension of the PEG chains and the attainment of a low molar mass dispersity (ranging from 1.03 to 1.07) (**Figure 5b, c**). To further distinguish the influence of the polypeptide molar mass from any influence of the secondary structure, we also analyzed the lyophilized powder obtained upon ROPISA using ATR-FTIR spectroscopy. The IR spectra of all copolymers, regardless of the size of the PEG component, exhibited β-sheet conformation, as evidenced by the presence of amide I and II peaks at 1630 cm^{-1} and at 1545 cm^{-1} (see **Figure S30, S40-S43**).

Overall, good control over the polymerization was achieved when initiated with PEG5k and PEG10k, demonstrating effective chain extension, no water initiation, and high yield. In contrast, the initiation with PEG2k showed less control, resulting in lower yields and higher average DPs than targeted. This suggests the potential hydrolysis of Phe-NCA into its corresponding amino acid, which was subsequently removed by dialysis. Notably, no evidence of water initiation was observed in this case.

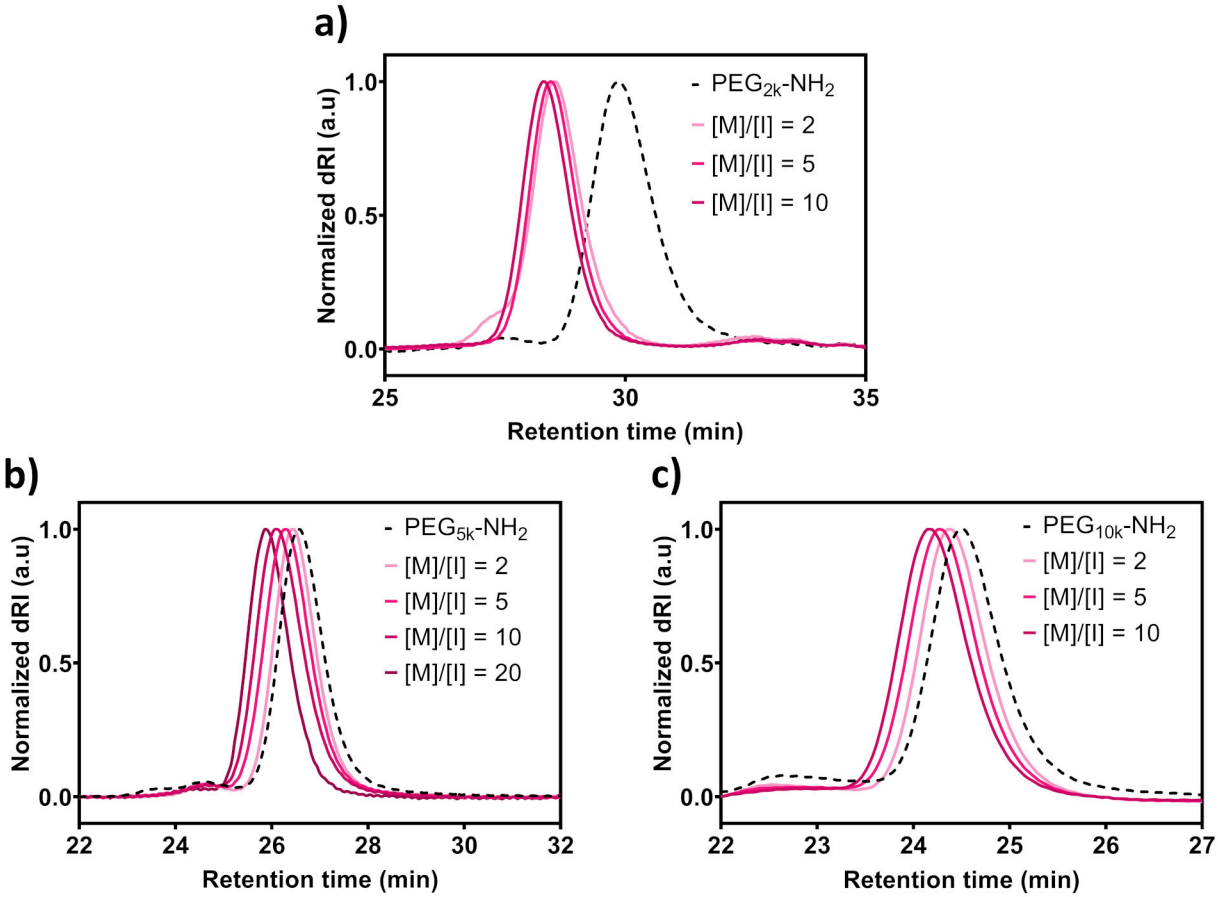

Figure 5. SEC profiles of (a) **PEG_{2k}-*b*-$PPhe_n$**, (b) **PEG_{5k}-*b*-$PPhe_n$** and (c) **PEG_{10k}-*b*-$PPhe_n$** with targeted DP of 2, 5, 10 and 20 in DMF + 1% LiBr.

Following dialysis against water to remove salts, the nanomaterial suspensions were also characterized using microscopy and light scattering techniques. DLS analysis confirmed the presence of nanoparticles with Z-average diameter ranging between 82 and 715 nm, with a relatively narrow size dispersity in the case of PEG_{5k} (**Table 2**, **Figure S44, S45**). Overall, TEM observations of the different suspensions indicated that the PEG fraction exerted a significant influence on the morphology of the nanoparticles. Representative TEM imaging is depicted in **Figure 6** as a function of PEG content or π–π stacking ability.

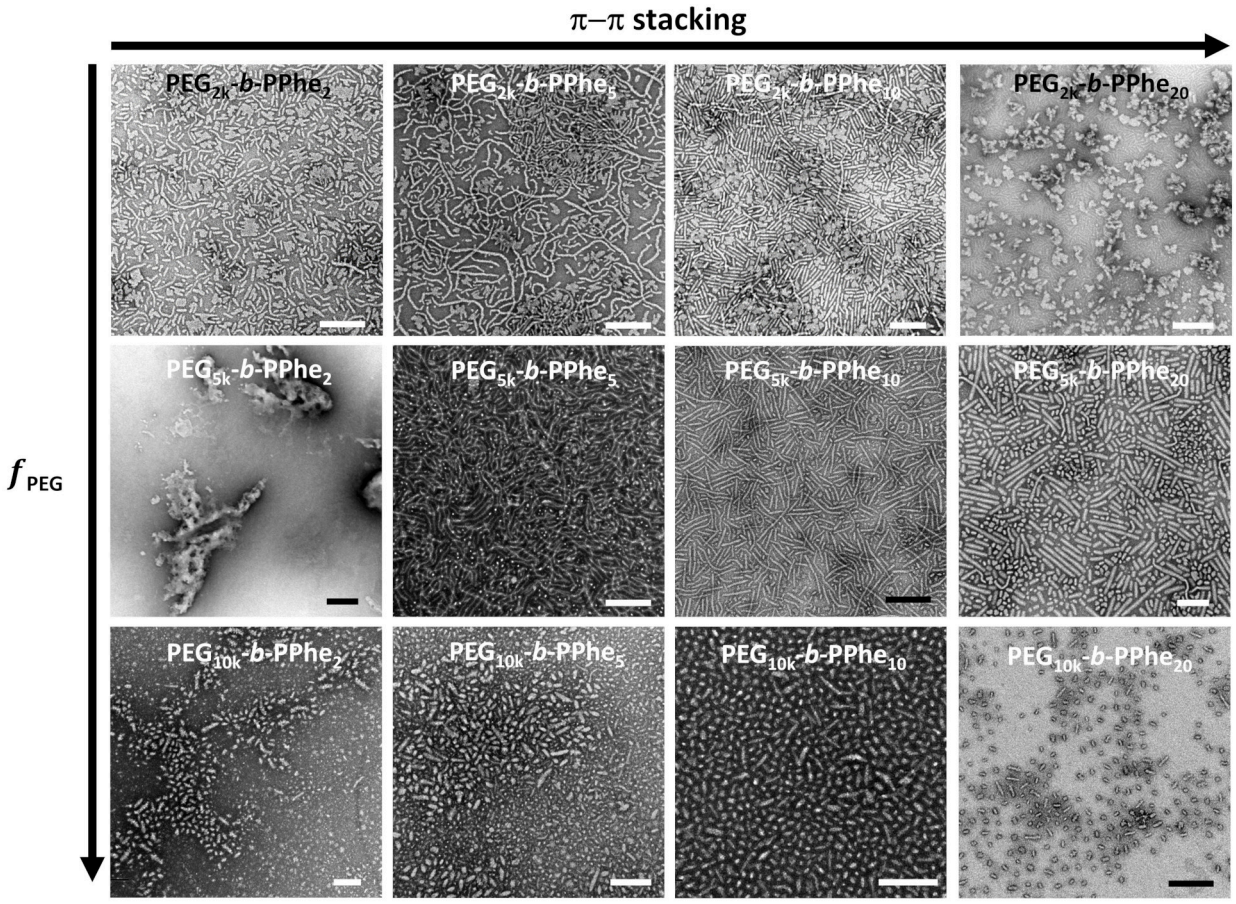

Figure 6. Representative TEM images of the different copolymer nanoparticles obtained with Phe, with different hydrophilic/hydrophobic block ratio and degree of π–π stacking (Scale-bar: 200 nm).

First, the addition of a longer polypeptide block and subsequent reduction of the hydrophilic fraction from 0.94 to 0.61 resulted in the formation of more rigid and thicker nanoparticles when PEG_{5k} was used (second line **Figure 6**). The **PEG_{5k}-*b*-$PPhe_5$** nanoparticles were characterized by a long, thin and flexible morphology. The **PEG_{5k}-*b*-$PPhe_{10}$** nanoparticles were thicker and more rigid, yet they were also mixed with shorter nanoparticles. With a lower PEG fraction value of 0.61, **PEG_{5k}-*b*-$PPhe_{20}$** exhibited thick and rigid structures but also mixed with spherical micelles. In comparison, when PEG_{10k} was used to increase the PEG fraction, the nanoparticles were of a shorter length and exhibited a markedly reduced degree of anisotropy. This phenomenon was attributable to the increased curvature that results from the larger hydrophilic PEG block and the higher hydrophilic fraction (0.73-0.96). Indeed, an increase in the hydrophilic block size enhances the surface area in contact with the aqueous environment, thereby facilitating the formation of more spherical or less elongated structures. In marked contrast, when the hydrophilic ratio was lower, as observed in the case of **PEG_{2k}-*b*-$PPhe_{20}$** (f_{PEG} = 0.48), resulting nanoparticles exhibited reduced anisotropy and aggregates

morphology. Additionally, despite having a similar hydrophilic fraction close to 0.75, **PEG_{10k}-*b*-$PPhe_{20}$** and **PEG_{5k}-*b*-$PPhe_{10}$** displayed distinct aspect ratio with more anisotropy arising from lower PEG molar mass. The ROPISA of phenylalanine, using poly(ethylene glycol) initiators of different molar masses, demonstrated that controlled polymerization could be achieved, leading to the formation of nanoparticles with different aspect ratios. In this context, the tuning of anisotropy is not solely dependent on the secondary structure (as beta-sheets are formed in all cases) or the monomer's hydrophobicity. It is also influenced by the hydrophilic/hydrophobic ratio and the π-π stacking interactions of phenylalanine. These findings highlight the potential of ROPISA as a powerful tool for generating anisotropic nanoparticles whose morphologies are tailored by various non-covalent interactions, including the use of monomers such as Phe-NCA, which are usually challenging to polymerize.

Towards more functional π-π interactions: Tyrosine NCA

In the field of nanomedicine, another NCA monomer of interest is derived from tyrosine, which shares similarities with phenylalanine. In contrast to phenylalanine, tyrosine possesses a polar side chain that undergoes a change in solubility when the pH of the solution exceeds the pKa of its phenol group. In drug-delivery, this specific feature enables the formation of strong π-π stacking and H-bonding interactions with drug molecules.[67,68] Aiming to design anisotropic nanomaterials made of this amino acid, a goal not yet achieved in literature, an in-depth study was conducted on the aqueous ROPISA of Tyrosine NCA and compared to phenylalanine. A series of block copolymers were synthesized by implementing the aqueous ROPISA using PEG_{5k}-NH_2 as the macroinitiator in an ice-cold aqueous sodium bicarbonate solution (pH 8.5, 50 mM) with 10, 20, 30, and 50 equivalents of Tyr-NCA monomer, while stirring vigorously. These stoichiometries were chosen to best cover the different PEG fractions, from 10 to 80% (see **Table 3**). It was noteworthy that for targeted DPs of 30 and 50, the aqueous medium exhibited a gradual gelation over time. The gelation ability of tyrosine in aqueous media has been previously investigated for its potential applications in biomedical fields, including drug delivery.[69–71] This encompasses the research conducted by *Huang* et al., who synthesized amphiphilic block copolymers based on PEG-*b*-(oligo)Tyr.[72] The previous research indicated that gelation properties were a result of the interaction between the polar phenolic side chains and the hydrophobic Tyr block.

Following purification, either from the gel or from the aqueous solution, the copolymers presented in table 3 were subjected to analysis by ^{1}H NMR and SEC. The results of the ^{1}H NMR spectroscopy revealed that the average number molar mass (M_n) values were in

agreement with the initial [M]/[I] ratio (**Table 3, Figure S13, S46**). However, the SEC chromatograms indicated that as the [M]/[I] ratio increases, there was a corresponding rise in the proportion of populations observed at higher retention times (**Figure S47**). We attributed this residual oligomer populations to water initiated polytyrosine that may have been produced by the gelation of the medium during ROPISA, which likely reduced the efficiency of monomer dispersion when stirring was ceased. We also conducted ATR-FTIR spectroscopy on the lyophilized powder obtained after ROPISA. All copolymers exhibited β-sheet conformation, an expected result, as evidenced by the presence of amide I and II peaks in their IR spectra (see (**Figure S31, S48**).

Table 3. Macromolecular characteristics of diblock copolymers obtained by aqueous ROPISA with Tyr-NCA.

Copolymer	Theory	SEC		^{1}H NMR			Yield (%)	DLS
	M_n [g.mol^{-1}]	M_n [g.mol^{-1}] [a]	$Đ$ [a]	M_n [g.mol^{-1}] [b]	DP [b]	f_{PEG} [c]		D_Z [nm] (σ) [d]
PEG$_{5k}$-*b*-PTyr$_{10}$	6 600	9 300	1.05	6 300	8	0.79	67	73 ± 3 (0.21 ± 0.01)
PEG$_{5k}$-*b*-PTyr$_{20}$	8 200	9 900	1.07	7 500	15	0.67	85	77 ± 4 (0.23 ± 0.1)
PEG$_{5k}$-*b*-PTyr$_{30}$	10 100	11 100	1.15	9 900	30	0.50	91	Gel
PEG$_{5k}$-*b*-PTyr$_{50}$	13 300	12 000	1.13	12 300	45	0.40	81	Gel
PEG$_{750}$-*b*-PTyr$_{20}$	3 900	3 300	1.46	4 300	22	0.14	85	Aggregates
PEG$_{2k}$-*b*-PTyr$_{20}$	5 200	5 500	1.13	5 300	20	0.46	84	560 ± 16 (0.21 ± 0.05)
PEG$_{10k}$-*b*-PTyr$_{20}$	13 300	22 200	1.06	17 700	47	0.56	46	441 ± 56 (0.75 ± 0.06)

[a] Number average molar-mass (M_n) and molar-mass dispersity determined by SEC in DMF +1% LiBr using PS calibration, [b] Number average molar-mass (M_n) and degree of polymerization (DP) determined by ^{1}H NMR in in DMSO-d_6, [c] Hydrophilic fraction or PEG fraction determined by this equation $\frac{M_n \text{ PEG}}{M_n \text{ copolymer}}$ with M_n from ^{1}H NMR.[d] Hydrodynamic diameter (D_Z) and polydispersity (σ) determined by DLS at 90°.

After dialysis against water to remove salts, the nanomaterial suspensions were characterized using TEM microscopy and light scattering techniques. Dynamic light scattering analysis of **PEG$_{5k}$-*b*-PTyr$_{10}$** and **PEG$_{5k}$-*b*-PTyr$_{20}$** revealed a close size distribution around 70 nm with a dispersity index of about 0.2 (**Figure S49**). However, TEM revealed that **PEG$_{5k}$-*b*-PTyr$_{10}$** formed spherical aggregates with an average diameter of 38 ± 8 nm (**Figure S49**) and **PEG$_{5k}$-*b*-PTyr$_{20}$** long and thin nanoparticles mixed with spherical micelles with an average length of 119 ± 83 nm and 12 ± 2 of diameter (**Figure S28**) as shown in **Figure 5**.

PEG$_{5k}$-*b*-PTyr$_{30}$ and **PEG$_{5k}$-*b*-PTyr$_{50}$** could not be analyzed by DLS due to gel formation. However, TEM analysis revealed the presence of non-homogeneous anisotropic nanoparticles, whose entanglement likely contributed to gel formation. These nanoparticles

exhibited dimensions of 113 ± 71 nm in length for the targeted DP of 30 and 61 ± 33 nm for the targeted DP of 50, with widths of 11 ± 2 nm and 17 ± 7 nm, respectively (**Figure 7, Figure S50-S52**).

Achieving anisotropy control and modulation with tyrosine proves to be challenging. Adjusting the feeding ratio during polymerization introduces additional complexities, including gel formation, which promotes water initiation and reduces control over polymerization. These factors result in less homogeneous self-assembled structures, highlighting the need for further optimization.

To better assess the influence of the PEG fraction, aqueous ROPISA was also attempted using PEG-NH_2 of different sizes, specifically 750 Da, 2 kDa, and 10 kDa, to vary the hydrophilic fraction as well as the number of tyrosine units (hydrophilic/hydrophobic ratio). ROPISA experiments were performed using ice-cold aqueous bicarbonate sodium buffer, with a feeding ratio of 20. Following the purification, ^{1}H NMR analysis was conducted, revealing that the DP values were close to the targeted one, with the exception of PEG_{10k} which exhibited a higher molar mass than the theoretical one (see **Table 3, Figure S53, S54**). In the SEC chromatograms, a shift to lower retention times confirmed the successful chain extension from the macroinitiator (**Figure S55**). **PEG_{750}-*b*-$PTyr_{20}$** displayed a rather high molar mass dispersity ($Đ$ = 1.46) as compared to the other copolymers but this result was attributed to the high dispersity of the commercial PEG_{750}-NH_2 used in this experiment ($Đ$ = 1.38). For **PEG_{10k}-*b*-$PTyr_{20}$**, the presence of tyrosine oligomers was observed, likely due to water-initiated polymerization of Tyr-NCA. At higher DP, NMR analyses indicated a loss in the control over the polymerization, confirming the SEC analyses. FTIR spectra revealed the presence β-sheet amide I and II bands for all the copolymers (**Figure S56**).

Following dialysis against water to remove salts, the nanomaterial suspensions were characterized using microscopy and light scattering techniques to assess the formation of anisotropic nanomaterials. **PEG_{750}-*b*-$PTyr_{20}$**, which has the lowest PEG fraction (f_{PEG} value of 0.14), displayed aggregates with a lamellar morphology in TEM (**Figure 7**). This morphology has already been reported by Jiang *et al.* with PEG_{2k}-*b*-$PTyr_{10}$ and upon nanoprecipitation.[73] Increasing the hydrophilic fraction while keeping the same targeted number of Tyr units appeared to stabilize the formation of elongated, heterogeneous nanoparticles, as observed by TEM and DLS. **PEG_{2k}-*b*-$PTyr_{20}$** nanoparticles (101 ± 51 nm, 15 ± 2 nm) were a bit thicker than PEG_{5k}-*b*-$PTyr_{20}$ (12 ± 2 nm) (**Figure 7, S28, S58**). For **PEG_{10k}-*b*-$PTyr_{20}$**, the nanoparticles were long and rigid but exhibited significant heterogeneity in length with a nanosheet morphology (see **Figure 7, S59**). The rigidity observed in the **PEG_{10k}-*b*-$PTyr_{20}$** nanoparticles could be due to strong π-π interactions among the tyrosine residues, but the

variation in their lengths suggests that the assembly process was not entirely uniform, possibly due to the lack of control during the ROPISA process.

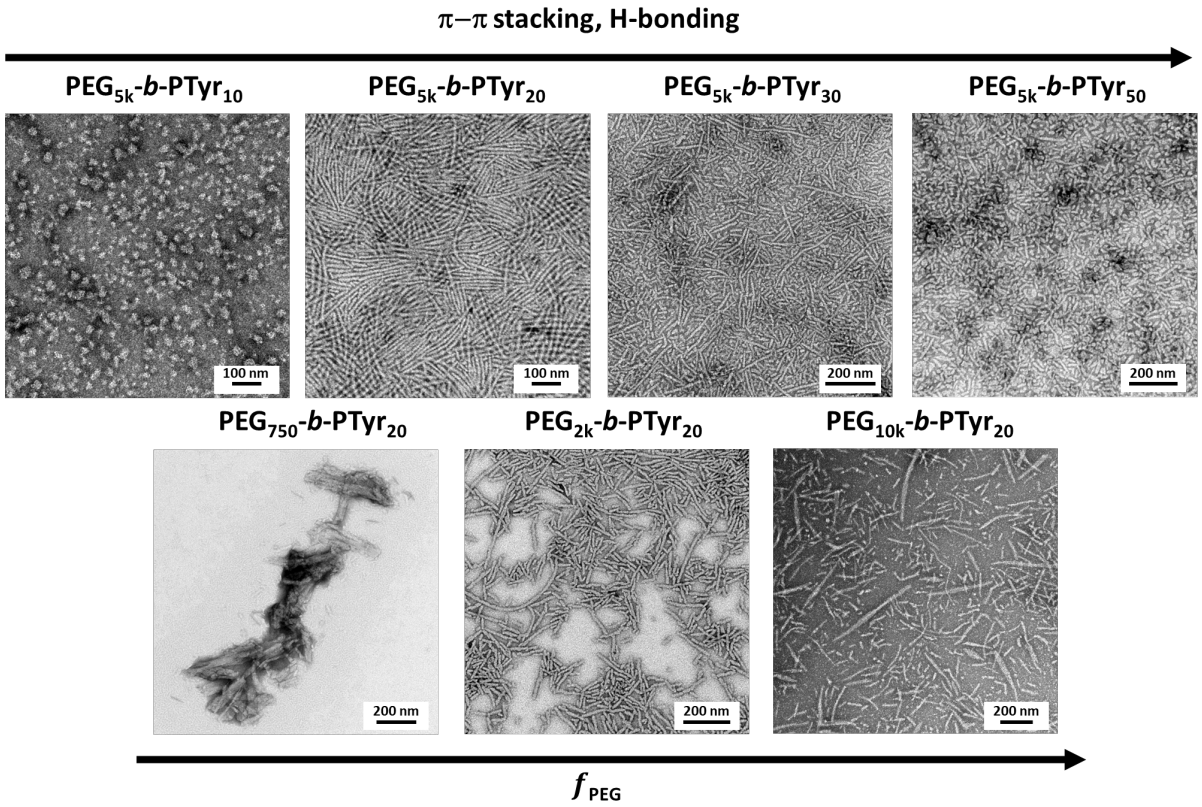

Figure 7. Representative TEM images of the different copolymer nanoparticles obtained with Tyr, with different hydrophilic/hydrophobic block ratio and degree of π–π stacking and H-bonding.

Overall, the aqueous ROPISA of Tyrosine NCA demonstrated that both the PEG fraction and the π–π stacking influenced the polymerization process and the anisotropy. Indeed, aqueous ROPISA performed with Tyrosine NCA afforded anisotropic nanomaterials with a complex influence of various factors, beyond the secondary structure, hydrophobicity, π-π stacking, and the hydrophilic/hydrophobic ratio. At higher M/I, water initiation and gel formation were observed but we found conditions in which a more pronounced anisotropic shape could be induced. Eventually, additional factors, such as hydrogen bonding ability and the amount of water-initiated polymerization could have also played a pivotal role in determining the final morphology, but these parameters were not studied in this work.

Conclusions

The synthesis of anisotropic nanoparticles by polymerization-induced self-assembly (PISA) remains a challenging process, yet it holds great promise to design drug-delivery systems. In this regard, the emerging use of aqueous ring-opening polymerization induced self-assembly (ROPISA) of *N*-carboxyanhydrides (NCAs) offers a promising strategy, enabling straightforward access to peptide-based nanomaterials. The present study was undertaken to evaluate the versatility of aqueous ROPISA across a range of NCAs, elucidating how their hydrophobicity and the chemical structure of the lateral chains provide access to nanoparticle anisotropy. In the initial phase of the study, lysine NCAs with Z, Boc, and TFA protecting groups were subjected to ROPISA. A more regulated aqueous polymerization and self-assembly was found for Lys(Z)-NCA, which results in a more uniform distribution of nanoparticles than that observed with Boc- and TFA-protected groups. Subsequently, to gain insight into the influence of side chain hydrophobicity, glycine, alanine, leucine and phenylalanine NCAs were subjected to further investigation. Interestingly, all these monomers produced anisotropic nanomaterials and we clearly observed that varying hydrophobicity but also π-π stacking or H-bonding ability impacted the kinetic of the ROP and the aspect ratio of the resulting nanomaterials. The incorporation of glycine, a hydrophilic monomer that polymerizes into a via hydrogen bonding, results in flexible fibrils due to its specific conformation. Nanoparticles derived from alanine exhibited greater anisotropy, which was attributed to a reduction in steric hindrance and a lower degree of hydrophobicity. The complexity of the system was increased by introducing phenylalanine, a more hydrophobic amino acid that promotes π-π stacking, which is of great interest in drug delivery. A comprehensive analysis was conducted by varying the size of both the hydrophilic poly(ethylene glycol) block and the hydrophobic polypeptide block, demonstrated that the hydrophilic/hydrophobic ratio and the number of phenylalanine units, which affect the extent of π-π stacking, had a significant impact on nanoparticle anisotropy. Similarly, the ability of tyrosine to influence nanoparticle morphology was examined, following the same approach used for phenylalanine. Tyrosine, with its phenol side chain, participates in π-π stacking and introduces hydrogen bonding, which is influenced by the pH of the medium. This property is advantageous in drug delivery applications as it potentially improves the drug loading contents due to these dual interactions. These interactions, in conjunction with the hydrophilic/hydrophobic equilibrium, were demonstrated to influence both the polymerization and self-assembly processes.

In summary, this study demonstrates the versatility and the robustness of aqueous ROPISA, a process that can be applied with almost all NCA monomers and its capacity to afford a wide range of tailored anisotropic nanoparticles. Most notably, it elucidates that factor such as hydrophobicity and steric hindrance, by influencing the polymerization kinetics, as well as π-π stacking,

hydrophilic/hydrophobic ratio, and hydrogen bonding serve as pivotal driving forces in regulating anisotropic self-assembly, in conjunction with secondary structure and monomer chirality.

Associated content

Supporting Information

The Supporting Information is available free of charge at http://pubs.acs.org.

Additional experimental details, including materials and method, synthetic protocols, kinetic studies; additional data, including ^{1}H NMR spectra, SEC chromatograms, ATR-FTIR spectra, DLS profiles and TEM images and histogram.

Author information

Corresponding Author

Sébastien Lecommandoux - *University Bordeaux, CNRS, Bordeaux INP, LCPO, UMR 5629, F-33600 Pessac, France.* https://orcid.org/0000-0003-0465-8603

Email : lecommandoux@enscbp.fr

Colin Bonduelle - *University Bordeaux, CNRS, Bordeaux INP, LCPO, UMR 5629, F-33600 Pessac, France.* https://orcid.org/0000-0002-7213-7861

Email : colin.bonduelle@enscbp.fr

Authors

Hannah Beauseroy- *University Bordeaux, CNRS, Bordeaux INP, LCPO, UMR 5629, F-33600 Pessac, France.* https://orcid.org/0009-0009-5961-9530

Fatemeh Salimi- *University Bordeaux, CNRS, Bordeaux INP, LCPO, UMR 5629, F-33600 Pessac, France.*

Julien Auchard-Catot- *University Bordeaux, CNRS, Bordeaux INP, LCPO, UMR 5629, F-33600 Pessac, France.*

Léna Alembik- *University Bordeaux, CNRS, Bordeaux INP, LCPO, UMR 5629, F-33600 Pessac, France.*

Author Contributions

The manuscript was written through contributions of all authors. All authors have given approval to the final version of the manuscript.

Notes

The authors declare no conflict of interest.

Acknowledgments

The authors acknowledge Amelie Vax and Sylvain Bourasseau for assistance with size-exclusion chromatography, Paul Marque for assistance with ATR-FTIR. This work was supported by a grant overseen by the French National Research Agency (ANR, Grant No. ANR-20-CE06-0020-01). This work was also conducted in the framework of the University of Bordeaux's IdEx "Investments for the Future" program RRI "Frontiel Of Life" that received financial support from the French government. This work was also supported by the Horizon Europe research and innovation program under the grant agreement No. 101079482 ("SUPRALIFE").

Graphical abstract

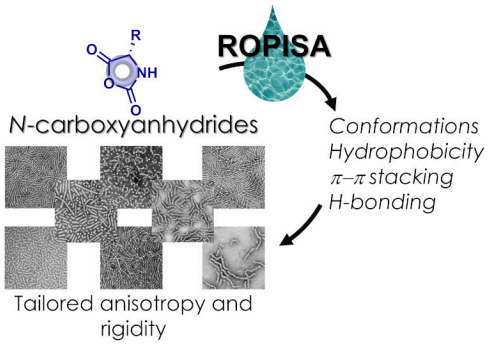

References

(1) Penfold, N. J. W.; Yeow, J.; Boyer, C.; Armes, S. P. Emerging Trends in Polymerization-Induced Self-Assembly. *ACS Macro Lett.* **2019**, *8* (8), 1029–1054. https://doi.org/10.1021/acsmacrolett.9b00464.

(2) Zhao, Z.; Lei, S.; Zeng, M.; Huo, M. Recent Progress in Polymerization-Induced Self-Assembly: From the Perspective of Driving Forces. *Aggregate* **2024**, *5* (1), e418. https://doi.org/10.1002/agt2.418.

(3) Takahashi, R.; Miwa, S.; Sobotta, F. H.; Lee, J. H.; Fujii, S.; Ohta, N.; Brendel, J. C.; Sakurai, K. Unraveling the Kinetics of the Structural Development during Polymerization-Induced Self-Assembly: Decoupling the Polymerization and the Micelle Structure. *Polym. Chem.* **2020**, *11* (8), 1514–1524. https://doi.org/10.1039/C9PY01810G.

(4) Czajka, A.; P. Armes, S. In Situ SAXS Studies of a Prototypical RAFT Aqueous Dispersion Polymerization Formulation: Monitoring the Evolution in Copolymer Morphology during Polymerization-Induced Self-Assembly. *Chemical Science* **2020**, *11* (42), 11443–11454. https://doi.org/10.1039/D0SC03411H.
(5) Derry, M. J.; Fielding, L. A.; Armes, S. P. Polymerization-Induced Self-Assembly of Block Copolymer Nanoparticles via RAFT Non-Aqueous Dispersion Polymerization. *Progress in Polymer Science* **2016**, *52*, 1–18. https://doi.org/10.1016/j.progpolymsci.2015.10.002.
(6) Warren, N. J.; Mykhaylyk, O. O.; Mahmood, D.; Ryan, A. J.; Armes, S. P. RAFT Aqueous Dispersion Polymerization Yields Poly(Ethylene Glycol)-Based Diblock Copolymer Nano-Objects with Predictable Single Phase Morphologies. *J. Am. Chem. Soc.* **2014**, *136* (3), 1023–1033. https://doi.org/10.1021/ja410593n.
(7) Ratcliffe, L. P. D.; Blanazs, A.; Williams, C. N.; Brown, S. L.; Armes, S. P. RAFT Polymerization of Hydroxy-Functional Methacrylic Monomers under Heterogeneous Conditions: Effect of Varying the Core-Forming Block. *Polym. Chem.* **2014**, *5* (11), 3643–3655. https://doi.org/10.1039/C4PY00203B.
(8) Blanazs, A.; Ryan, A. J.; Armes, S. P. Predictive Phase Diagrams for RAFT Aqueous Dispersion Polymerization: Effect of Block Copolymer Composition, Molecular Weight, and Copolymer Concentration. *Macromolecules* **2012**, *45* (12), 5099–5107. https://doi.org/10.1021/ma301059r.
(9) Guild, J. D.; Knox, S. T.; Burholt, S. B.; Hilton, Eleanor. M.; Terrill, N. J.; Schroeder, S. L. M.; Warren, N. J. Continuous-Flow Laboratory SAXS for In Situ Determination of the Impact of Hydrophilic Block Length on Spherical Nano-Object Formation during Polymerization-Induced Self-Assembly. *Macromolecules* **2023**, *56* (16), 6426–6435. https://doi.org/10.1021/acs.macromol.3c00585.
(10) Li, Z.; Wang, R.; Luo, X.; Zhang, L.; Tan, J. ABC or ACB Triblock Copolymers? Changing the RAFT Group Position in Diblock Copolymer Macro-RAFT Agents Leads to Different PISA Behaviors in RAFT Dispersion Polymerization. *Polym. Chem.* **2024**, *15* (17), 1736–1747. https://doi.org/10.1039/D3PY01330H.
(11) Gao, C.; Li, S.; Li, Q.; Shi, P.; Shah, S. A.; Zhang, W. Dispersion RAFT Polymerization: Comparison between the Monofunctional and Bifunctional Macromolecular RAFT Agents. *Polym. Chem.* **2014**, *5* (24), 6957–6966. https://doi.org/10.1039/C4PY01069H.
(12) Zhang, X.; Rieger, J.; Charleux, B. Effect of the Solvent Composition on the Morphology of Nano-Objects Synthesized via RAFT Polymerization of Benzyl Methacrylate in Dispersed Systems. *Polym. Chem.* **2012**, *3* (6), 1502–1509. https://doi.org/10.1039/C2PY20071F.
(13) Zhou, D.; Dong, S.; P. Kuchel, R.; Perrier, S.; B. Zetterlund, P. Polymerization Induced Self-Assembly: Tuning of Morphology Using Ionic Strength and pH. *Polymer Chemistry* **2017**, *8* (20), 3082–3089. https://doi.org/10.1039/C7PY00552K.
(14) Boissé, S.; Rieger, J.; Pembouong, G.; Beaunier, P.; Charleux, B. Influence of the Stirring Speed and CaCl $_2$ Concentration on the Nano-object Morphologies Obtained via RAFT-mediated Aqueous Emulsion Polymerization in the Presence of a Water-soluble macroRAFT Agent. *J. Polym. Sci. A Polym. Chem.* **2011**, *49* (15), 3346–3354. https://doi.org/10.1002/pola.24771.
(15) Ding, Z.; Gao, C.; Wang, S.; Liu, H.; Zhang, W. Macro-RAFT Agent Mediated Dispersion Polymerization: The Monomer Concentration Effect on the Morphology of the in Situ Synthesized Block Copolymer Nano-Objects. *Polym. Chem.* **2015**, *6* (46), 8003–8011. https://doi.org/10.1039/C5PY01202C.
(16) Parkinson, S. J.; Fielden, S. D. P.; Thomas, M.; Miller, A. J.; Topham, P. D.; Derry, M. J.; O'Reilly, R. K. Harnessing Cytosine for Tunable Nanoparticle Self-Assembly Behavior Using Orthogonal Stimuli. *Biomacromolecules* **2024**, *25* (8), 4905–4912. https://doi.org/10.1021/acs.biomac.4c00352.
(17) Wan, W.-M.; Pan, C.-Y. Formation of Polymeric Yolk/Shell Nanomaterial by Polymerization-Induced Self-Assembly and Reorganization. *Macromolecules* **2010**, *43* (6), 2672–2675. https://doi.org/10.1021/ma100021a.
(18) Hochreiner, E. G.; van Ravensteijn, B. G. P. Polymerization-Induced Self-Assembly for Drug Delivery: A Critical Appraisal. *Journal of Polymer Science* **2023**, *61* (24), 3186–3210. https://doi.org/10.1002/pol.20230579.
(19) Lages, M.; Nicolas, J. In Situ Encapsulation of Biologically Active Ingredients into Polymer Particles by Polymerization in Dispersed Media. *Progress in Polymer Science* **2023**, *137*, 101637. https://doi.org/10.1016/j.progpolymsci.2022.101637.
(20) Phan, H.; Cossutta, M.; Houppe, C.; Le Cœur, C.; Prevost, S.; Cascone, I.; Courty, J.; Penelle, J.; Couturaud, B. Polymerization-Induced Self-Assembly (PISA) for in Situ Drug Encapsulation or Drug

Conjugation in Cancer Application. *Journal of Colloid and Interface Science* **2022**, *618*, 173–184. https://doi.org/10.1016/j.jcis.2022.03.044.
(21) Pearce, A. K.; Wilks, T. R.; Arno, M. C.; O'Reilly, R. K. Synthesis and Applications of Anisotropic Nanoparticles with Precisely Defined Dimensions. *Nat Rev Chem* **2021**, *5* (1), 21–45. https://doi.org/10.1038/s41570-020-00232-7.
(22) Truong, N. P.; Quinn, J. F.; Whittaker, M. R.; Davis, T. P. Polymeric Filomicelles and Nanoworms: Two Decades of Synthesis and Application. *Polym. Chem.* **2016**, *7* (26), 4295–4312. https://doi.org/10.1039/C6PY00639F.
(23) Geng, Y.; Dalhaimer, P.; Cai, S.; Tsai, R.; Tewari, M.; Minko, T.; Discher, D. E. Shape Effects of Filaments versus Spherical Particles in Flow and Drug Delivery. *Nature Nanotech* **2007**, *2* (4), 249–255. https://doi.org/10.1038/nnano.2007.70.
(24) Hadji, H.; Bouchemal, K. Effect of Micro- and Nanoparticle Shape on Biological Processes. *Journal of Controlled Release* **2022**, *342*, 93–110. https://doi.org/10.1016/j.jconrel.2021.12.032.
(25) Zeeshan, A.; Hadji, H.; Khelifa, H.; Bourge, M.; Bouchemal, K. Understanding the Interplay between Surface Properties and the Aspect Ratio of Ellipsoidal Nanomaterials. *Colloids and Surfaces A: Physicochemical and Engineering Aspects* **2024**, *680*, 132680. https://doi.org/10.1016/j.colsurfa.2023.132680.
(26) Rieger, J. Guidelines for the Synthesis of Block Copolymer Particles of Various Morphologies by RAFT Dispersion Polymerization. *Macromolecular Rapid Communications* **2015**, *36* (16), 1458–1471. https://doi.org/10.1002/marc.201500028.
(27) Kang, Y.; Pitto-Barry, A.; Willcock, H.; Quan, W.-D.; Kirby, N.; Sanchez, A. M.; O'Reilly, R. K. Exploiting Nucleobase-Containing Materials – from Monomers to Complex Morphologies Using RAFT Dispersion Polymerization. *Polym. Chem.* **2014**, *6* (1), 106–117. https://doi.org/10.1039/C4PY01074D.
(28) Yu, Q.; Ding, Y.; Cao, H.; Lu, X.; Cai, Y. Use of Polyion Complexation for Polymerization-Induced Self-Assembly in Water under Visible Light Irradiation at 25 °C. *ACS Macro Lett.* **2015**, *4* (11), 1293–1296. https://doi.org/10.1021/acsmacrolett.5b00699.
(29) Yoon, K.-Y.; Lee, I.-H.; Kim, K. O.; Jang, J.; Lee, E.; Choi, T.-L. One-Pot in Situ Fabrication of Stable Nanocaterpillars Directly from Polyacetylene Diblock Copolymers Synthesized by Mild Ring-Opening Metathesis Polymerization. *J. Am. Chem. Soc.* **2012**, *134* (35), 14291–14294. https://doi.org/10.1021/ja305150c.
(30) Boott, C. E.; Gwyther, J.; Harniman, R. L.; Hayward, D. W.; Manners, I. Scalable and Uniform 1D Nanoparticles by Synchronous Polymerization, Crystallization and Self-Assembly. *Nature Chem* **2017**, *9* (8), 785–792. https://doi.org/10.1038/nchem.2721.
(31) Huo, M.; Song, G.; Zhang, J.; Wei, Y.; Yuan, J. Nonspherical Liquid Crystalline Assemblies with Programmable Shape Transformation. *ACS Macro Lett.* **2018**, *7* (8), 956–961. https://doi.org/10.1021/acsmacrolett.8b00409.
(32) Wan, J.; Fan, B.; Thang, S. H. RAFT-Mediated Polymerization-Induced Self-Assembly (RAFT-PISA): Current Status and Future Directions. *Chem. Sci.* **2022**, *13* (15), 4192–4224. https://doi.org/10.1039/D2SC00762B.
(33) Wang, Y.; Lorandi, F.; Fantin, M.; Matyjaszewski, K. Atom Transfer Radical Polymerization in Dispersed Media with Low-Ppm Catalyst Loading. *Polymer* **2023**, *275*, 125913. https://doi.org/10.1016/j.polymer.2023.125913.
(34) Delaittre, G.; Nicolas, J.; Lefay, C.; Save, M.; Charleux, B. Surfactant-Free Synthesis of Amphiphilic Diblock Copolymer Nanoparticles via Nitroxide-Mediated Emulsion Polymerization. *Chem. Commun.* **2005**, No. 5, 614–616. https://doi.org/10.1039/B415959D.
(35) Foster, J. C.; Varlas, S.; Couturaud, B.; Jones, J. R.; Keogh, R.; Mathers, R. T.; O'Reilly, R. K. Predicting Monomers for Use in Polymerization-Induced Self-Assembly. *Angewandte Chemie International Edition* **2018**, *57* (48), 15733–15737. https://doi.org/10.1002/anie.201809614.
(36) Ikkene, D.; Six, J.-L.; Ferji, K. Progress in Aqueous Dispersion RAFT PISA. *European Polymer Journal* **2023**, *188*, 111848. https://doi.org/10.1016/j.eurpolymj.2023.111848.
(37) Shen, D.; Shi, B.; Zhou, P.; Li, D.; Wang, G. Temperature-Dependent Ring-Opening Polymerization-Induced Self-Assembly Using Crystallizable Polylactones as Core-Forming Blocks. *Macromolecules* **2023**. https://doi.org/10.1021/acs.macromol.3c00681.

(38) Hurst, P. J.; Rakowski, A. M.; Patterson, J. P. Ring-Opening Polymerization-Induced Crystallization-Driven Self-Assembly of Poly-L-Lactide-Block-Polyethylene Glycol Block Copolymers (ROPI-CDSA). *Nat Commun* **2020**, *11* (1), 1–12. https://doi.org/10.1038/s41467-020-18460-2.
(39) Ellis, C. E.; Garcia-Hernandez, J. D.; Manners, I. Scalable and Uniform Length-Tunable Biodegradable Block Copolymer Nanofibers with a Polycarbonate Core via Living Polymerization-Induced Crystallization-Driven Self-Assembly. *J. Am. Chem. Soc.* **2022**, *144* (44), 20525–20538. https://doi.org/10.1021/jacs.2c09715.
(40) Jiang, J.; Zhang, X.; Fan, Z.; Du, J. Ring-Opening Polymerization of N-Carboxyanhydride-Induced Self-Assembly for Fabricating Biodegradable Polymer Vesicles. *ACS Macro Lett.* **2019**, *8* (10), 1216–1221. https://doi.org/10.1021/acsmacrolett.9b00606.
(41) Grazon, C.; Salas-Ambrosio, P.; Ibarboure, E.; Buol, A.; Garanger, E.; Grinstaff, M. W.; Lecommandoux, S.; Bonduelle, C. Aqueous Ring-Opening Polymerization-Induced Self-Assembly (ROPISA) of N-Carboxyanhydrides. *Angewandte Chemie International Edition* **2020**, *59* (2), 622–626. https://doi.org/10.1002/anie.201912028.
(42) Shi, Q.; Chen, Y.; Yang, J.; Yang, J. Ring-Opening Polymerization-Induced Self-Assembly (ROPISA) of Salicylic Acid o -Carboxyanhydride. *Chemical Communications* **2021**, *57* (86), 11390–11393. https://doi.org/10.1039/D1CC04630F.
(43) Grazon, C.; Salas-Ambrosio, P.; Antoine, S.; Ibarboure, E.; Sandre, O.; Clulow, A. J.; Boyd, B. J.; Grinstaff, M. W.; Lecommandoux, S.; Bonduelle, C. Aqueous ROPISA of α-Amino Acid N-Carboxyanhydrides: Polypeptide Block Secondary Structure Controls Nanoparticle Shape Anisotropy. *Polym. Chem.* **2021**, *12* (43), 6242–6251. https://doi.org/10.1039/D1PY00995H.
(44) Bartlett, P. D.; Jones, R. H. A Kinetic Study of the Leuchs Anhydrides in Aqueous Solution. I1. *J. Am. Chem. Soc.* **1957**, *79* (9), 2153–2159. https://doi.org/10.1021/ja01566a035.
(45) Bartlett, P. D.; Dittmer, D. C. A Kinetic Study of the Leuchs Anhydrides in Aqueous Solution. II1. *J. Am. Chem. Soc.* **1957**, *79* (9), 2159–2160. https://doi.org/10.1021/ja01566a036.
(46) Beauseroy, H.; Grazon, C.; Antoine, S.; Badreldin, M.; Salas-Ambrosio, P.; Harrisson, S.; Garanger, E.; Lecommandoux, S.; Bonduelle, C. Polypeptide- and Protein-Based Conjugate Nanoparticles via Aqueous Ring-Opening Polymerization-Induced Self-Assembly (ROPISA). *Macromolecular Rapid Communications* **2024**, *45* (14), 2400079. https://doi.org/10.1002/marc.202400079.
(47) Morrell, A. H.; Warren, N. J.; Thornton, P. D. The Production of Polysarcosine-Containing Nanoparticles by Ring-Opening Polymerisation-Induced Self-Assembly. *Macromolecular Rapid Communications* **2024**, 2400103. https://doi.org/10.1002/marc.202400103.
(48) Tinajero-Díaz, E.; Judge, N.; Li, B.; Leigh, T.; Murphy, R. D.; Topham, P. D.; Derry, M. J.; Heise, A. Poly(l-Proline)-Stabilized Polypeptide Nanostructures via Ring-Opening Polymerization-Induced Self-Assembly (ROPISA). *ACS Macro Lett.* **2024**, 1031–1036. https://doi.org/10.1021/acsmacrolett.4c00400.
(49) Liu, B.; Fang, R.; Li, W.; Wu, X.; Liu, T.; Lin, M.; Sun, J.; Chen, X. Fast Catalyst-Free Synthesis of Stereoselective Polypeptides via Hierarchical Chiral Assembly. *J. Am. Chem. Soc.* **2024**, *146* (24), 16558–16566. https://doi.org/10.1021/jacs.4c03281.
(50) Xi Huang, S.; Hao Wang, Z.; Lin, M.; Hui Fu, X.; Sun, J. One-Pot Preparation of Polypeptide Nanogels in Aqueous Solution via Ring-Opening Polymerization-Induced Nano-Gelation. *Polymer Chemistry* **2023**, *14* (15), 1801–1808. https://doi.org/10.1039/D3PY00206C.
(51) Tian, L.; Cao, C.; Ho, J.; Stenzel, M. H. Maximizing Aqueous Drug Encapsulation: Small Nanoparticles Formation Enabled by Glycopolymers Combining Glucose and Tyrosine. *J. Am. Chem. Soc.* **2024**, *146* (12), 8120–8130. https://doi.org/10.1021/jacs.3c12502.
(52) Isidro-Llobet, A.; Álvarez, M.; Albericio, F. Amino Acid-Protecting Groups. *Chem. Rev.* **2009**, *109* (6), 2455–2504. https://doi.org/10.1021/cr800323s.
(53) Rodríguez-Hernández, J.; Gatti, M.; Klok, H.-A. Highly Branched Poly(l-Lysine). *Biomacromolecules* **2003**, *4* (2), 249–258. https://doi.org/10.1021/bm020096k.
(54) Gavva, V.; Al Musaimi, O.; Bent, C.; Williams, D. R. Determining the Hydrophobicity Index of Protected Amino Acids and Common Protecting Groups. *Separations* **2023**, *10* (8), 456. https://doi.org/10.3390/separations10080456.
(55) Mozhaev, V. V.; Berezin, I. V.; Martinek, K.; Nosoh, Y. Structure-Stability Relationship in Proteins: Fundamental Tasks and Strategy for the Development of Stabilized Enzyme Catalysts for Biotechnolog. *Critical Reviews in Biochemistry* **1988**, *23* (3), 235–281. https://doi.org/10.3109/10409238809088225.

(56) *Calculation of molecular properties and bioactivity score*. https://www.molinspiration.com/cgi/properties (accessed 2025-01-11).
(57) Karandur, D.; Wong, K.-Y.; Pettitt, B. M. Solubility and Aggregation of Gly5 in Water. *J. Phys. Chem. B* **2014**, *118* (32), 9565–9572. https://doi.org/10.1021/jp503358n.
(58) Bykov, S.; Asher, S. Raman Studies of Solution Polyglycine Conformations. *J. Phys. Chem. B* **2010**, *114* (19), 6636–6641. https://doi.org/10.1021/jp100082n.
(59) Lotz, B. Rippled Sheets: The Early Polyglycine Days and Recent Developments in Nylons. *ChemBioChem* **2022**, *23* (5), e202100658. https://doi.org/10.1002/cbic.202100658.
(60) Taga, K.; Sowa, M. G.; Wang, J.; Etori, H.; Yoshida, T.; Okabayashi, H.; Mantsch, H. H. FT-IR Spectra of Glycine Oligomers. *Vibrational Spectroscopy* **1997**, *14* (1), 143–146. https://doi.org/10.1016/S0924-2031(96)00061-6.
(61) Hurst, P. J.; Graham, A. A.; Patterson, J. P. Gaining Structural Control by Modification of Polymerization Rate in Ring-Opening Polymerization-Induced Crystallization-Driven Self-Assembly. *ACS Polym Au* **2022**, *2* (6), 501–509. https://doi.org/10.1021/acspolymersau.2c00027.
(62) Palermo, N. Y.; Csontos, J.; Murphy, R. F.; Lovas, S. The Role of Aromatic Residues in Stabilizing the Secondary and Tertiary Structure of Avian Pancreatic Polypeptide. *Int J Quantum Chem* **2008**, *108* (4), 814–819. https://doi.org/10.1002/qua.21521.
(63) Lanzarotti, E.; Biekofsky, R. R.; Estrin, D. A.; Marti, M. A.; Turjanski, A. G. Aromatic-Aromatic Interactions in Proteins: Beyond the Dimer. *J Chem Inf Model* **2011**, *51* (7), 1623–1633. https://doi.org/10.1021/ci200062e.
(64) Liu, X.; Fan, R.; Lu, B.; Le, Y. Polypeptides Micelles Composed of Methoxy-Poly(Ethylene Glycol)-Poly(l-Glutamic Acid)-Poly(l-Phenylalanine) Triblock Polymer for Sustained Drug Delivery. *Pharmaceutics* **2018**, *10* (4), 230. https://doi.org/10.3390/pharmaceutics10040230.
(65) Bossion, A.; Nicolas, J. Synthesis of Poly(Asparagine-Co-Phenylalanine) Copolymers, Analogy with Thermosensitive Poly(Acrylamide-Co-Styrene) Copolymers and Formation of PEGylated Nanoparticles. *European Polymer Journal* **2020**, *140*, 110033. https://doi.org/10.1016/j.eurpolymj.2020.110033.
(66) Aydinlioglu, E.; Abdelghani, M.; Le Fer, G.; van Hest, J. C. M.; Sandre, O.; Lecommandoux, S. Robust Polyion Complex Vesicles (PICsomes) Based on PEO-b-Poly(Amino Acid) Copolymers Combining Electrostatic and Hydrophobic Interactions: Formation, siRNA Loading and Intracellular Delivery. *Macromolecular Chemistry and Physics* **2023**, *224* (1), 2200306. https://doi.org/10.1002/macp.202200306.
(67) Gu, X.; Qiu, M.; Sun, H.; Zhang, J.; Cheng, L.; Deng, C.; Zhong, Z. Polytyrosine Nanoparticles Enable Ultra-High Loading of Doxorubicin and Rapid Enzyme-Responsive Drug Release. *Biomater. Sci.* **2018**, *6* (6), 1526–1534. https://doi.org/10.1039/C8BM00243F.
(68) Gu, X.; Wei, Y.; Fan, Q.; Sun, H.; Cheng, R.; Zhong, Z.; Deng, C. cRGD-Decorated Biodegradable Polytyrosine Nanoparticles for Robust Encapsulation and Targeted Delivery of Doxorubicin to Colorectal Cancer *in Vivo*. *Journal of Controlled Release* **2019**, *301*, 110–118. https://doi.org/10.1016/j.jconrel.2019.03.005.
(69) Bastiat, G.; Plourde, F.; Motulsky, A.; Furtos, A.; Dumont, Y.; Quirion, R.; Fuhrmann, G.; Leroux, J.-C. Tyrosine-Based Rivastigmine-Loaded Organogels in the Treatment of Alzheimer's Disease. *Biomaterials* **2010**, *31* (23), 6031–6038. https://doi.org/10.1016/j.biomaterials.2010.04.009.
(70) Costache, M. C.; Vaughan, A. D.; Qu, H.; Ducheyne, P.; Devore, D. I. Tyrosine-Derived Polycarbonate-Silica Xerogel Nanocomposites for Controlled Drug Delivery. *Acta Biomater* **2013**, *9* (5), 6544–6552. https://doi.org/10.1016/j.actbio.2013.01.034.
(71) Tiwari, P.; Basu, A.; Sahu, S.; Gound, S.; Christman, R. M.; Tiwari, A. K.; Trivedi, P.; DuttKonar, A. An Auxin–Tyrosine Derivative Based Biocompatible Supergelator: A Template for Fabrication of Nanoparticles for Sustained Release of Model Drugs. *New J. Chem.* **2018**, *42* (7), 4915–4922. https://doi.org/10.1039/C7NJ04390B.
(72) Huang, J.; Hastings, C. L.; Duffy, G. P.; Kelly, H. M.; Raeburn, J.; Adams, D. J.; Heise, A. Supramolecular Hydrogels with Reverse Thermal Gelation Properties from (Oligo)Tyrosine Containing Block Copolymers. *Biomacromolecules* **2013**, *14* (1), 200–206. https://doi.org/10.1021/bm301629f.
(73) Jiang, C.; Zhao, C.; Xu, P.; Song, Q.; Tao, X.; Lin, S. Effects of Secondary Structures and pH on the Self-Assembly of Poly(Ethylene Glycol)-b-Polytyrosine. *Biomacromolecules* **2024**. https://doi.org/10.1021/acs.biomac.4c00437.